People's Democratic Republic of Algeria
Ministry of Higher Education and Scientific Research

University M'Hamed BOUGARA – Boumerdes

Institute of Electrical and Electronic Engineering

Department of Power and Control

Final Year Project Report Presented in Partial Fulfilment of the Requirements for the Degree of

MASTER

In **Electrical and Electronic Engineering**

Option: **Power Engineering**

Title:

PC based online Platform for PV module characterization and ODM parameters identification

Presented by:

ZEMMOURI Radia

Supervisor:

Pr. BENTARZI Hamid

ABSTRACT

A low cost frame work using PC based platform associated with LabVIEW program has been developed to obtain the current-voltage (I-V) and power-voltage (P-V) curves automatically. This developed platform uses the Arduino board to acquire the measured current, voltage, temperature, and irradiance from the PV panel under test using different sensors such as current transformer, thermistor and irradiance transducer.

The new developed platform can provide the dynamic parameters such as maximum power and its corresponding voltage and current with high accuracy and precision in measurement under different environmental conditions. It stores the measured data for the objective of identification and extraction the five electrical parameters of the PV module's one diode mathematical model using grey wolf optimizer.

Dedication

I dedicate this work

To my parents.

To my brother Rabie and sisters Yasmine and Ilhem.

To all my family members for their encouragements.

To the memory of my grandmother

and my uncle Ibrahim.

To everyone who loves me and everyone I love.

Radia Zemmouri

ACKNOWELEDJMENT

{AND MY SUCCESS IS NOT BUT THROUGH ALLAH,

UPON HIM I HAVE RELIED, AND TO HIM I RETURN}

HUD: 88

I send my deep sense of gratitude and thankfulness to my academic supervisor Pr.Bentarzi Hamid for the guidance and kindness, for everything he did during the realization of this work and during the two Master's years.

I extend my thanks to all the professors of the Institute of Electrical and Electronic Engineering.

A special thanks to everyone who contributed in this work from near or far especially Ms.Touabi.

TABLE OF CONTENTS

CHAPTER 3
INSTRUMENTATIONS AND METHODS

CHAPTER 4
TEST RESULTS

CHAPTER 5
CONCLUSION AND FUTURE RESEARCH

LIST OF FIGURES

LIST OF TABLES

LIST OF ABBREVIATIONS

ABBREVIATION	DEFINITION
PV	Photo-Voltaic
UV	Ultra-Violet
IV	Infra-Red
GSR	Global Solar Radiation
AM	Air Mass
C-SI	Crystalline Silicon
PN	Positive-Negative
MPP	Maximum Power Point
CdTe	Cadmium Telluride
a-Si	Amorphous Silicon
Rs	Series Resistance
Rsh	shunt Resistance
STC	Standard Test Conditions
ODM	One Diode Model
KCL	Kirchhoff's current law
LIFA	LabVIEW Interface For Arduino
NOCT	Nominal Operating Cell Temperature
DC	Direct Current
USB	Universal Serial Bus
PCB	Printed Circuit Board
3D	Three-Dimensions
1D	One-Dimension
DAQ	Data AQuisitin
GWO	Grey Wolf Optimization
VI	Virtual Instrument
BD	Block Diagram
FP	Front Panel
PC	Personal Computer

LIST OF SYMBOLS

SYMBOL	DESCRIPTION	UNIT
I	Current	A
V	Voltage	V
P	Power	W
Iph	Photo-generated current	A
n	Ideality factor	-
Is	Saturated current	A
Rs	Series resistance	OHM
Rsh	Shunt resistance	OHM
T	Temperature	°C or K
G	Irradiance	W/m^2
Voc	Open-circuit voltage	V
Isc	Short circuit current	A
Vm	Maximum voltage	V
Im	Maximum current	A
Pm	Maximum power	W
AM	Air mass	-

1

GENERAL INTRODUCTION

1.1 Overview

Electricity is the life-blood to our planet since ancient times. It facilitates technological advancements and underpins a wide range of products and services that illuminate the world and stimulate economical and industrial productivity.

Electric power generation is mainly based on conventional fossil sources and nuclear power in many countries, among them Algeria that contributed in 2016 with about 98.75% of its fossil fuels in electricity supply. Consequently, as much as power demand increases, a shortfall is expected in providing these non-renewable fuels which include oil, coal and natural gas, and a serious growth in environmental pollution and global warming due to the release of carbon dioxide (CO_2), nitrous oxide (N_2O), methane (CH_4) and other greenhouse gases.

In 2020 Algeria ranked the third large (CO_2) producer in Africa with around 155 million metric tons of carbon dioxide emissions, and one of the top seven gas flaring countries according to the World Bank's global gas flaring reduction partnership. For those reasons, immediate actions were required to start showing some interest in renewable energies that can replace conventional sources and give a new breath to the world and the environment. Renewable energies are the clean energies that will deliver solutions that help the world to meet its inhabitance health and environmental protection in an increasingly affordable way. They are characterized by their availability, sustainability, low consumption of resources, compatibility with the climate, riskless energy production, and low-cost while reducing pollution and creating job opportunities. The energy from the sun is truly immense, so it can satisfy all these requirements of a sustainable energy supply today and in the future. Therefore, the scientists discovered the photovoltaic effect and then started installing the different photovoltaic systems (grid-connected, stand-alone, and hybrid). These systems have the ability to convert solar energy into applicable and clean electricity. Consequently, with the increasing demand for continuous power supply, optimizing the photovoltaic conversion process has led to many studies, one of them is to analyze and obtain photovoltaic characteristics at different temperature and irradiance levels. This can permit for online monitoring of the different results and thus developing ways to enhance the efficiency and the PV parameters.

1.2 Motivation

"Civilization will be mostly solar-powered in the future", the tweet of the Tesla CEO Elon Musk on Twitter, which affirms that the world has changed course towards renewable energies that will move the future. For this reason, researches and studies are accelerating to improve and create new technologies that will raise the efficiency of the PV panels and thus solar systems. However, this research provides a real-time characterization of the PV modules under different environmental conditions and online estimation of the PV panel mathematical model parameters.

1.3 Objectives

The main objectives of this project are:

- Design and implement a LabVIEW-Arduino based real-time data acquisition system to collect the experimental characteristics of a photovoltaic module under different temperature and irradiance levels.
- Develop a LabVIEW based optimizer to extract and estimate the five electrical parameters of the one diode mathematical model of the PV module using the experimental acquired data from the LabVIEW-Arduino system.

1.4 Outlines

The report is organized as follows:

- The first chapter presents an overview and a motivation to work on this topic.
- The second chapter deals with a theoretical literature about solar radiation and photovoltaic effect.
- The third chapter describes the instruments utilized to implement this PC based data acquisition system for PV module characterization and the developed program using the LabVIEW. Besides, the method grey wolf optimizer that has been used to identify the ODM electrical parameters.
- The fourth chapter presents the experimental findings using the developed data acquisition system and the grey wolf optimizer.
- The fifth chapter gives a general conclusion.

2

BACKGROUND IN THE SOLAR RADIATION AND PHOTOVOLTAIC CONVERSION

2.1 Introduction

Solar energy striking the Earth's surface is so vast that in less than one hour can provide a year of daily supplied power that can satisfy the energy demand of the human population. [1] This solar power is converted into applicable electricity employing photovoltaic systems. Supplementary details about solar radiation and photovoltaic conversion are introduced in this chapter.

2.2 Solar Radiation

2.2.1 Solar radiation emitted by the Sun

2.2.1.1 Sun

The Sun is the center of the solar system. It is a ball of hot plasma and glowing gases. Three-quarters of the Sun's mass consists of Hydrogen H2 (75%), the rest is Helium He (23%) and other heavier elements (02%), Including Carbon (C), Oxygen (O2), and Iron (Fe). [2] The Sun is the closest star to the Earth that travels around it in an oval-shaped orbit that is known as the Earth's ellipse. Therefore, the planet's distance from the Sun varies throughout the year. However, the average distance is about 150 million kilometers. [3] Sun releases an enormous amount of energy of 4.10^{26}W through continuous and active thermonuclear reactions inside its core. This power is evacuated to the outside in the form of electromagnetic radiations by its peripheral surface whose temperature is 5900 K. [4]

2.2.1.2 Solar radiation

Radiation from the Sun is the energy in the form of rays and electromagnetic waves. For illustration, (**Fig. 2.1**) shows that the radiations can be seen (visible light) or felt (infrared radiations) and other forms like X-rays and gamma rays [5]. The power of solar radiations emitted in the space is about 64.10^3 KW/m^2. The radiation diffuses and travels all over the space with light speed (300000 Km/s). The average energy flux incident on a unit area perpendicular to the external Earth's surface is 1367 W/m^2, which is called the solar constant [1].

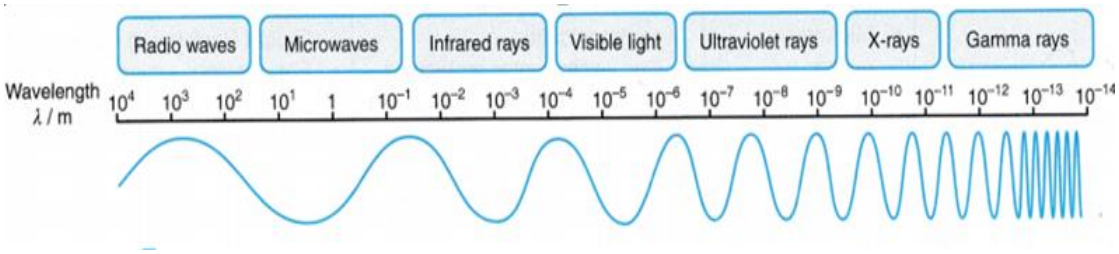

Figure 2.1 Electromagnetic Radiations

2.2.1.3 Solar spectrum

Sun emits electromagnetic radiations from gamma rays to radio waves. However, the spectral irradiance intensity varies with the radiation wavelength. The peak of the spectrum of the Sun-ray just outside the entry into the Earth's atmosphere is within the visible light and some significant amounts of shorter and longer wavelengths (UV and IR respectively), (**Fig.2.2**). Eventually, 92.2% of the solar energy radiated and carried into electromagnetic waves reaches the Earth's atmosphere, and it is distributed as follows: 8.2% of UV radiation, 40.9% of visible light, and 50.8% are by IR radiations. [6]

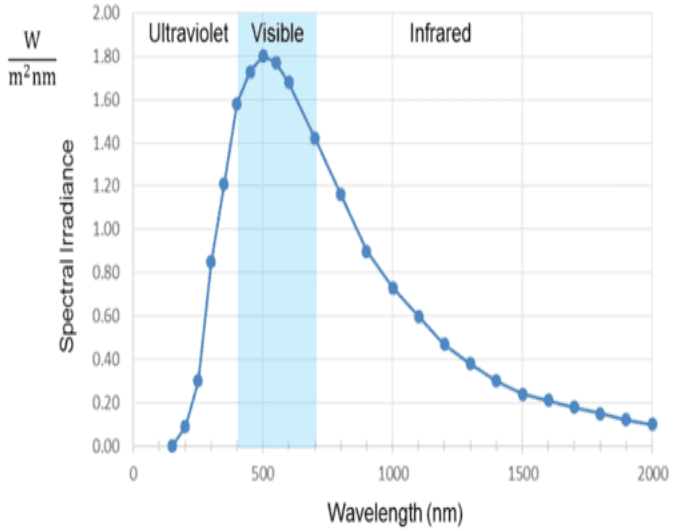

Figure 2.2 Solar spectrum

2.2.2 Solar radiation propagated in the atmosphere

Global solar radiation is an essential parameter in meteorology, renewable energy and for the design and operation of solar energy systems. The GSR reaches Earth's surface as:

direct, diffuse and reflected radiations (**Fig.2.3**).

2.2.2.1 Solar radiation affecting materials

As solar radiation penetrates the Earth's atmosphere, it will be subjected to a number of interactions. A part of the incident radiation will reflect and return back to its primary medium, this radiation is neglected. The amount of radiation that reaches the Earth’s ground is either diffused in all directions due to microscopic particles or absorbed by materials. The absorbed energy has a direct impact on the electronic excitation of some devices like solar cells, and their temperature.

2.2.2.2 Atmospheric constituents affecting solar radiation

Less than 51% of the total radiations generated by the Sun reach the Earth's surface due to the atmospheric scattering and absorption that affect the intensity and the spectral composition of the available radiation.

- Atmospheric scattering is the unpredictable diffusion of radiation by the small particles (dust and aerosols) and gas molecules that diffuse an incoming radiation in random directions without affecting its wavelength. [7]
- Atmospheric absorption of certain photons results in the effective loss of energy to atmospheric constituents and gases (CO_2, O_2, water vapor and ozone O_3) at given wavelengths.

However, the rest of solar radiation from the Sun is reflected back to space when it strikes the clouds.

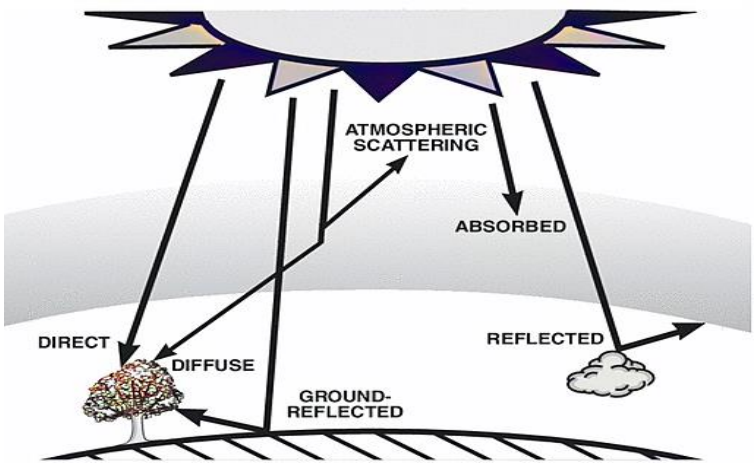

Figure 2.3 Global solar radiation

(Source: Newport, Introduction to Solar Radiation)

2.2.2.3 Atmosphere affecting solar radiation

The amount of the incident solar radiation on the Earth's ground is extremely variable due to some atmospheric conditions that have a direct impact on the intensity of the received radiation, such as the ground level, water vapor, and the zenith angle. However, the effect of the atmosphere on sunlight is identified as the Air Mass which corresponds to the length of the direct sunrays path through the atmosphere; it is a suitable concept to study the atmosphere's effect on the solar spectrum and its intensity [1]. On a clear summer day at sea level and the Sun is overhead, the direct sunlight at zenith passes through the atmosphere without interruptions, and it corresponds to the air mass 1 direct (AM1D) spectrum. When the

extraterrestrial spectrum passes through no atmosphere is called the air mass zero (AM0) radiation. The air mass corresponds to the crossing of an atmosphere and a half (AM1.5) with a total irradiance of 1000 W/m^2; it is used for the calibration of solar cells. The air mass for other times is equal to $\frac{1}{\cos \theta z}$, where θz is the zenith angle that corresponds to the angle between the position of the Sun and the Horizon (**Fig.2.4**).[1]

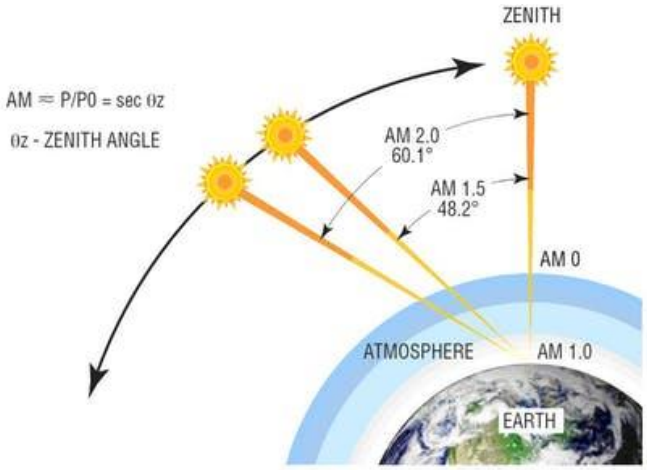

Figure 2.4 Optical Air Mass

2.2.3 Solar radiation received by the globe

After a long travel from the Sun and penetrating the atmosphere, the sunlight radiation reaches the Earth's ground. But its intensity will not remain constant all over the world. Besides, the atmospheric conditions, the geographical location of some areas, and the change in the Sun's position affect directly the amount of the incident sunlight.

2.2.3.1 Geographical location

The round shape of the Earth makes the irradiance of the incident sunlight highly dependent on the latitude. The areas that lie near the equator and are located between the tropics that are for latitudes from - 23.5 to + 23.5 receive the highest irradiance in the year when the sun is directly overhead at 90^0 with respect to the earth's surface. **Fig.2.5** illustrates that the Mediterranean regions that are located approximately at 23^0 northern latitude receive an irradiance up to 3000 KWh /m^2 [8]. As the distance from the equator gets vaster, the Sun gets at minimum angles and then the solar energy received is least. Whereas, the areas at the poles and for latitudes above 66.5^0 receive no solar irradiance for days.[9]

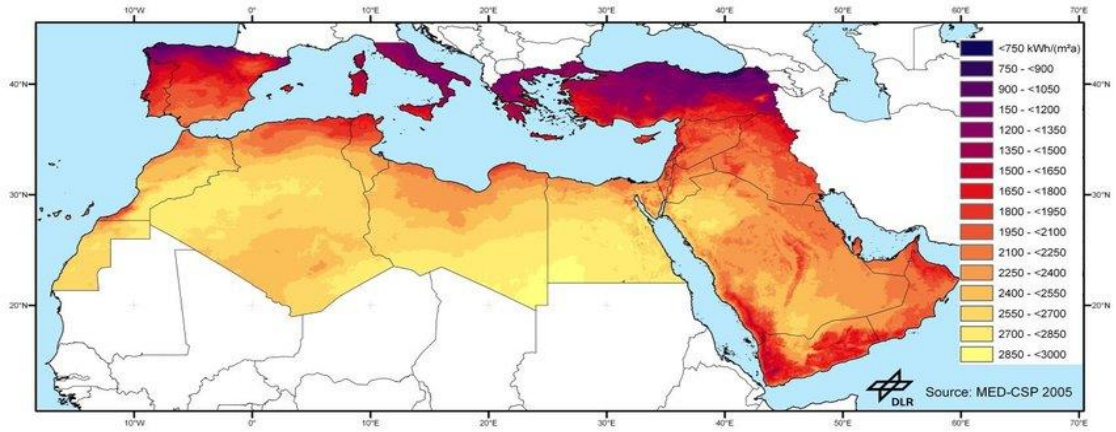

Figure 2.5 Annual Direct Solar Irradiance [kWh/m²] in the Mediterranean countries and on the Arabic peninsula (Source: DLR, 2005)

2.2.3.2 Sun-Earth position

The total solar irradiance is defined as the function between the irradiance of the emissions and the mean Earth-Sun distance. Due to the rotation of the Earth every 23 hours and 56 minutes around its own axis that is slightly tilted at an angle of 23.5^0, varying amounts of radiation are received at different times. Consequently, the position of the Earth and Sun over the course of approximately 24-hours-rotation causes sunrise, sunset, day and night. Moreover, the regular revolution of the Earth around the Sun in an elliptical orbit causes the annual variation of irradiance during the different seasons. In January, the Earth is about 3% closer to the Sun (~ 5 million km), then the Sun's ray hits the Earth at a shallow angle. These radiations are more spread out which minimizes the amount of energy reaching any spot. While in early July, the Earth is further about 3% from the Sun which makes the radiation hits the Earth at a steep angle. Thus, the light does not spread much out which maximizes the energy reaching any spot.

2.2.3.3 Solar radiation measurements

During the operation of a photovoltaic system, data about solar irradiance and solar insolation are required since they have a direct impact on the power produced. Different equipments are used to measure the direct, diffuse and global solar radiation periodically throughout the day.

- **Global solar radiation**

The incident global solar radiation is measured using the pyranometer that uses the thermopile principal. The incident radiation is absorbed by the horizontal black surface that converts the received energy into heat that will be experienced on the thermocouple module located beneath the black body. The difference in the temperature between one side and another of the thermocouple sensor is proportional to the irradiance of the global radiation and this difference is converted into readable data (voltage) and then into irradiance amount (**Fig.2.6**).[10]

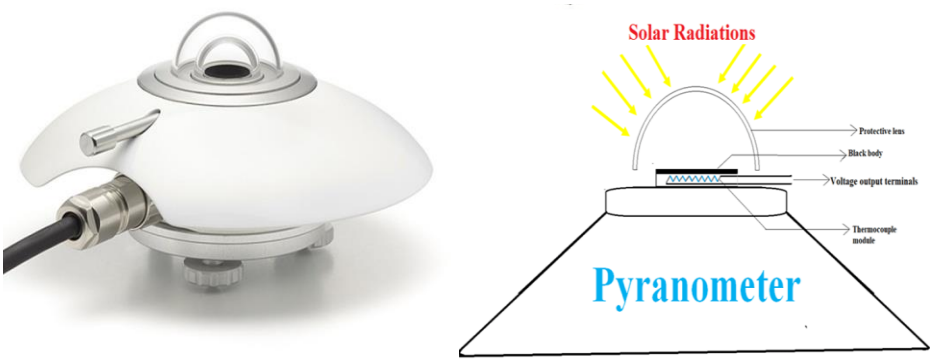

Figure 2.6 Pyranometer

- **Diffuse solar radiation**

It is measured using the pyranometer by shading the direct sunlight and letting the thermocouple module receives only the diffuse radiations (**Fig.2.7**).

Figure 2.7 Pyranometer with a shadow ring

- **Direct solar radiation**

Direct sunlight is measured using Pyrheliometer that consists of a protective lens at the top of a tube, and a black body and a thermocouple sensor at its base with a viewing angle of 5^0 which limits the incident radiation to direct only. As the black body absorbs the radiation, the temperature rises and then will be sensed by the thermocouple module that induces a voltage between its terminal and thus the irradiance of the direct beam radiation is measured. For a

continuous readings of the direct radiation irradiance, the pyrheliometer is integrated with a Sun tracker to keep the instrument aimed at Sun (**Fig.2.8**).[10]

Figure 2.8 Pyrheliometer

2.3 Photovoltaic Conversion

2.3.1 Introduction

Producing electricity has relied upon fossil fuel derivatives for years to satisfy the high daily demand for electric power which created an obvious impasse in providing electric energy and fuels in particular, whereby the prices are rising continuously. Alternatives are found to guarantee a continuous energy supply and preserve the climate and the environment. Besides, this energy must be provided free of risks and with low costs to avoid military conflicts on energy resources and additional environmental pollution. Solar photovoltaic has been one of the pioneering renewable technologies that convert solar power into usable electricity.

At the end of 2020, the total solar photovoltaic installed capacity in the world amounted to 773.2 GW, with an increase of 127 GW (+22%), representing the third-largest renewable energy source after hydropower and wind accounting for 2799 GW and 733 GW of capacity, respectively. (Source: International renewable energy agency IRENA, 2021)

2.3.2 Solar cells technology

The generator of a photovoltaic installation is the PV panels that are connected together in such a way to supply energy; each panel is composed of a number of semiconductor materials that produce electricity once they are exposed to the sunlight. These devices are solar cells.

2.3.2.1 Silicon

Most solar cells available in the market are made up of Silicon semiconductor due to its photovoltaic properties. It provides a path for electron-hole circulation within it and its chemical composition that can be slightly modified to optimize its electrical properties. Moreover, Silicon makes up 27.7% of the Earth's crust; it is the second most abundant element in nature being surpassed by Oxygen. However, it does not exist in a pure form but is combined with Oxygen forming a compound called Silica or Silicon Dioxide (SiO_2) besides other forms. To increase its purity so it can be used for electronic applications the "Siemens process" is applied to form the polycrystalline silicon in a solid form with purity of 99.99999%. [1] ,[11]

2.3.2.2 Doping process

Another process is required to re-shape the produced Silicon semiconductor ingots into cylindrical or square forms that are sliced then into wafers **(Fig. 2.9**). These wafers are experienced to the thermal diffusion process in a high-temperature furnace (~1100^0C) by adding specific types of impurity atoms; this doping process aims to change the conductivity type of the semiconductor and alter its electrical characteristics. However, the extrinsic Silicon semiconductor can be of N-type with large electron concentration than holes due to adding pentavalent atoms such as Phosphorus (^{15}P) that has five valence electrons to the Silicon atoms (^{14}Si). The opposite holds for adding trivalent dopant atoms such that the Boron (^{5}B) with three valence electrons producing a majority of holes and minority of electrons.[12]

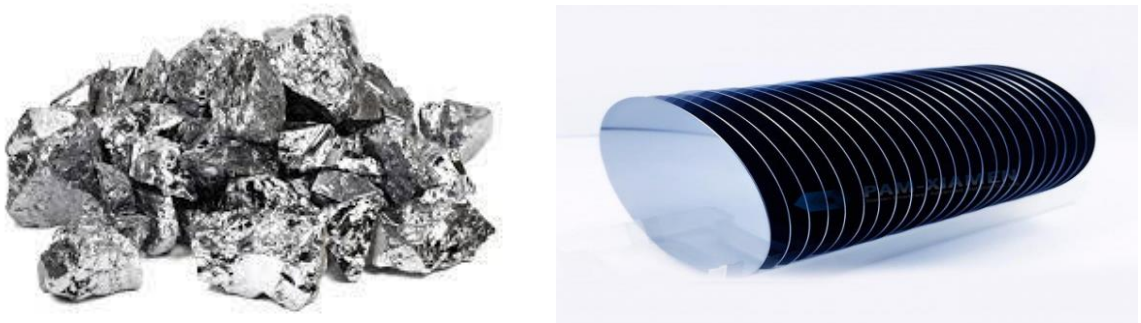

Figure 2.9 From a Silicon rock to wafers

2.3.2.3 Crystalline silicon solar cell

The PN junction of a solar cell is formed when a part of the cell is already doped negatively and then the remaining surface will be exposed to Boron atoms to produce P-type Silicon. When the P and N layers are created, they provide a path for electrons and holes to recombine together creating a hard barrier of electron-hole pairs at the junction. However, an electric field is caused between the positive and negative ions in the depletion region preventing the migration of electrons on the N-side to the P-side. The simple structure of the C-Si solar cell is shown in (**Fig.2.10**). Both sides of the wafer are highly doped forming an emitter layer (n^+-type) at the top and an absorber (p^+- type) at the bottom that generates and transports the charge carriers while the P-type layer at the rear region is to decrease the chances of carriers recombination at the back surface. The conductive matrix at the top of the wafer is used to provide a limited distance for electrons to go through the Silicon. In addition to the anti-reflection coating that is utilized to eliminate the optical reflections and increase light transmission on the solar cell. [13]

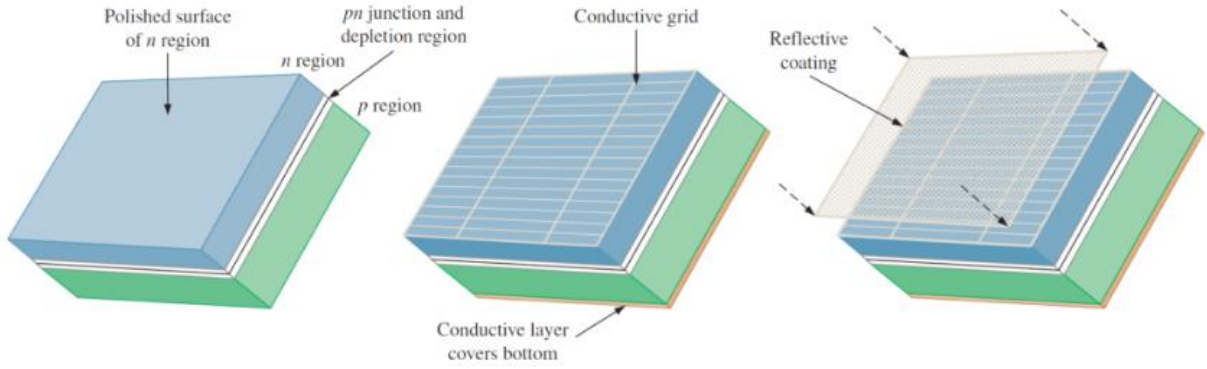

Figure 2.10 Solar cell structure

2.3.2.4 The different photovoltaic technologies

Single crystal Silicon solar cell was the first technology put in use for space applications in 1958 with an efficiency of 6%. This cell is still the dominant and most effective technology in the market due to the simplest structure, acceptable efficiency and low-cost. The energy crisis in the last decades accelerated the researches to develop new technologies for the terrestrial applications. Some changes are applied on the fabrication procedures and the design of the crystalline cells to reduce the cost and use less-refined silicon. [14] The two types of the C-Si are:

- **Polycrystalline silicon solar cells**

They are made of many different Silicon fragments that are melted together to form a molten Silicon liquid that will be cooled down and solidified into cubic-shaped blocks. The resulting ingots are cut into thin square wafers with less-uniform colored look due to the effect of the different crystalographic orientations (**Fig.2.11.a**).

- **Monocrystalline silicon solar cells**

During the fabrication process of the single crystalline solar cells, the pure Silicon ingots with a cone shape are sliced to form square thin layers with rounded corners to minimize the waste materials. Therefore, the resulting monocrystalline cell has a uniform dark look that is due to the pure silicon utilized (**Fig.2.11.b**).

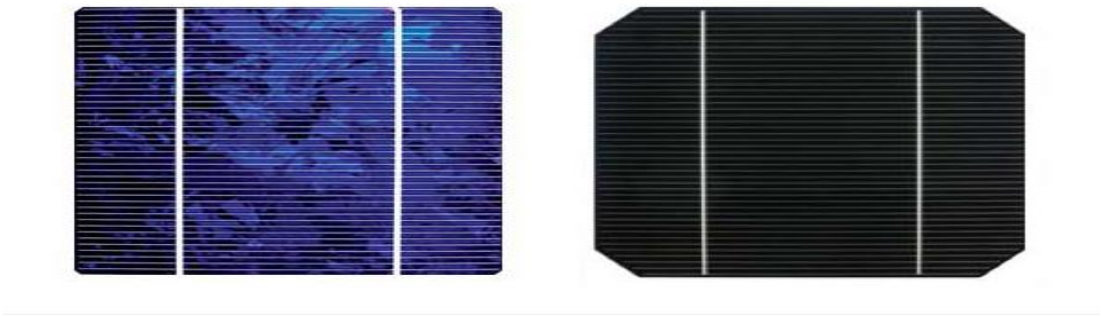

(a) **(b)**

Figure 2.11 (a) Polycrystalline silicon solar cells; (b) Monocrystalline silicon solar cells

The second generation of the solar cells is the thin films. They are developed to decrease the material costs of the crystalline Silicon cells and provide an acceptable and an efficient conversion of the solar energy. Different materials are used in the fabrication process of the thin film solar cells such as: copper indium diselenide (CIs), cadmium telluride (CdTe), hydrogenerated amorphous silicon (a-Si:H) and others. **Table.2.1** presents an overview of the different solar cell technologies.

	1st generation		2nd generation	
Material	polycrystalline	monocrystalline	CdTe	a-Si
Industrial efficiency	10-15%	12-20%	8-11%	5-7%
Temperature coefficient	-0.4 to -0.5%/C^0		-0.25%/C^0	-0.21%/C^0
Lifespan	25-30years		>25years	~10years
Commercia-lization	85-00%		In researches	90-100%

Table.2.1 Comparison between the different solar cell technologies

2.3.3 Photovoltaic effect

The working principle of a photovoltaic cell is to generate a potential difference at the junction in response to visible or other radiation, this is called the photovoltaic effect.

2.3.3.1 Solar cell absorbs the light

The electromagnetic waves that interact with the solar cell as discrete amounts are called photons, and as they strike the PN junction an electron is released. The energy needed to free an electron from its valence band is the band-hole energy which is equal to 1.12 electron-volts for silicon atoms. However, each photon can free only one electron at each time which results in a free hole, and the excess energy of some photons will be wasted as heat in the cell. The generation of the electron-hole pairs in both sides of the semiconductor results in an increase of the number of minority charge carriers. The free electrons are repelled away from the p-side towards the positive potential of the n-side, and the same for the holes by the internal electric field created in the depletion region. If the solar cell is connected to an external circuit, then the electrons will flow from the n-side into the connecting wire through the load and back to the p-side to recombine with the holes (**Fig.2.12**). Therefore, the photovoltaic conversion is about converting the energy in the sunlight into usable direct current.

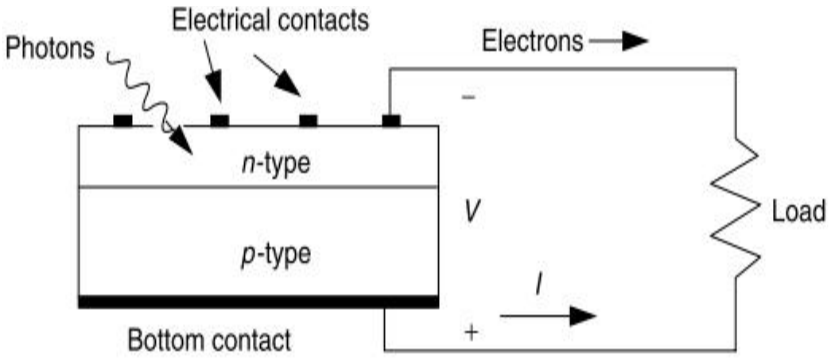

Figure 2.12 Photovoltaic effect

2.3.4 Mathematical model of the PV cell

The mathematical model is a basic tool of the real system simulation and an efficient way to describe the electrical behavior of electronic devices. Moreover,it facilities the complex physical process using a simple equivalent circuit. There are many models for PV cells: the single-diode and the double-diode models are the most commonly used in the description of photovoltaic cell's working principle. [15][16]

2.3.4.1 Single-diode model

The simplest and most used equivalent circuit for a non-ideal photovoltaic cell is the one-diode model (**Fig.2.13**) that describes diffusion and recombination characteristics of the charge carriers in the semiconductor [17]. It consists of the following electrical components:

- Current source that corresponds to the developed photocurrent that depends on the solar irradiance and the temperature of the cell.
- Diode shunted with the current source to model the PN junction effect of the solar cell.
- Series resistor with a small resistance is used to describe the bulk resistance of the semiconductor material, the contact resistance between the metal contact and the interconnectors, and the resistance of the top and rear metal contacts.[18]
- Shunt resistor with a large resistance represents the power losses in the solar cell due to the leakage current path from the light generated current. The effect of R_{sh} is severe at low light levels due to the less-light generated current. [18]

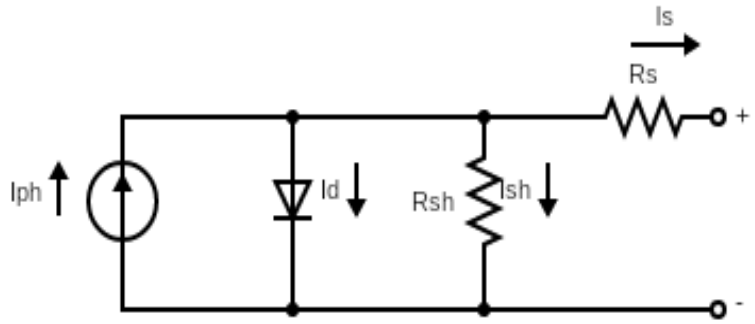

Figure 2.13 Single-diode model

Applying Kirchhoff's current law (KCL) in the single-diode model in **Fig.2.13**, the output current of the PV cell is: [19]

$$\boldsymbol{I = Iph - Id - Ish} \tag{2.1}$$

Where,

$\boldsymbol{Iph}$ is the photo-generated current, $\boldsymbol{Id}$ is the diode current, $\boldsymbol{Ish}$ is the current through ***Rsh***.

The photo current is described as: [15]

$$\boldsymbol{Iph = Iscr\frac{G}{Gstc}[1 + K1(T + Tstc)]} \tag{2.2}$$

Where,

- $\boldsymbol{Iscr}$: The reference short circuit current (from the data sheet).
- ***G:*** The actual solar isolation [w/m^2]
- ***Gstc=1KW/m2***: solar irradiance under standard test conditions.
- ***K1:*** Cell's short circuit current temperature coefficient.
- ***T:*** Cell's temperature.
- $\boldsymbol{Tstc=25^0C}$

The diode current is given by the equation:

$$\boldsymbol{Id = Is\left[e^{\frac{V+Is.Rs}{nVtNs}} - 1\right]} \tag{2.3}$$

Where,

- ***Is:*** *The* saturation current of the cell, $Is=CT^3e^{\frac{Egap}{KT}}$, with $Egap=1.12ev$, the band gap of the semiconductor, $C=T/Tstc$, the temperature coefficient, and $K=1.38.10^{-23}\ J/K$, the Boltzman constant.
- ***Vt*:** The thermal voltage, $Vt=\frac{KT}{q}$, with $q=1.6.10^{-19}C$, the electron's charge, and ***T:*** The ambient temperature.
- $n=[1,2]$, the ideality factor of the diode.
- ***Ns:*** number of solar cells in series.

Shunt current is given as:

$$Ish=\frac{V+IsRs}{Rsh} \tag{2.4}$$

Therefore, the mathematical equation that describes the non-ideal behavior of a real photovoltaic module is given as:

$$I=Iph-Is\left[e^{\frac{V+I.Rs}{nVtNs}}-1\right]-\frac{V+I.Rs}{Rsh} \tag{2.5}$$

2.3.4.2 Double-diode model

The two-diode model in (**Fig.2.14**) with 2 diodes with different ideality factors are connected in parallel to provide accurate results compared with the one-diode model, especially when the irradiance gets lower. Besides the description of the diffusion and recombination characteristics of the charge carriers, it models the recombination in space charge zone. [15][17].

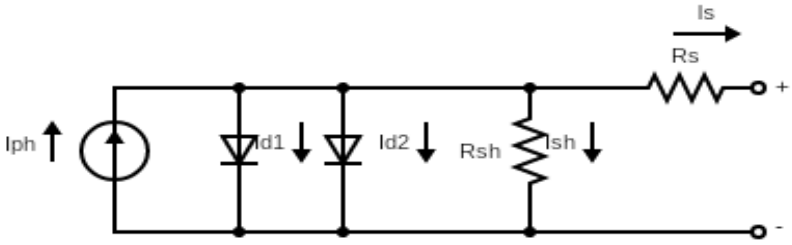

Figure 2.14 Double-diode model.

The mathematical equations that describe the two-diode model can be derived from Kirchhoff's low:

$$I=Iph-Id1-Id2-Ish \tag{2.6}$$

$$I = Iph - Is1\left[e^{\frac{V+I.Rs}{n1Vt1Ns}} - 1\right] - Is2\left[e^{\frac{V+I.Rs}{n2Vt2Ns}} - 1\right] - \frac{V+I.Rs}{Rsh} \quad (2.7)$$

2.3.5 Photovoltaic characteristics

The performance of a photovoltaic cell is said to be efficient if the PV cell provides an effective and robust light to electricity conversion. The main parameters that are used to plot the l-V and P-V curves are: the short-circuit current (Isc), and the open-circuit voltage (Voc).Therefore, the fill-factor and the efficiency parameters can be derived.

- **Short-circuit current Isc :**

The short circuit current is the current that flows through the external circuit when the positive and negative electrodes of the cell are short-circuited. The (Isc) represents the maximum current that can be delivered by the PV cell when there is no voltage. However, it is influenced by the optical properties that are standardized according to the STC to 1KW/m^2 and 1.5 AM Spectrum. [14]

- **Open-circuit voltage Voc:**

The open circuit voltage is the induced voltage across the external terminals of the PV cell when no load is connected, and no flow of current. (Voc) represents the maximum voltage that can be delivered by a cell.

- **Fill-factor FF :**

The fill-factor is an essential parameter that measures the maximum power and describes the quality of a designed solar cell. [19] The FF is the ratio between the maximum theoretical power and the measured maximum power, as given in equation (2.8):

$$FF = \frac{ImpVmp}{IscVoc} \quad (2.8)$$

Under the optimum and ideal conditions, the FF is closer to1. However, for real-time operation the FF falls in the range of 0.5 to 0.82.

Conversion efficiency η :

The efficiency is the most important parameter in the solar cell theory. It describes the amount of conversion of sunlight into electricity, and is defined as the ratio between the actual generated power and the actual incident radiation energy as shown in equation (2.9).

However, the light energy is usually obtained using standard test conditions under 1.5 AM spectrum.

$$\eta = \frac{ImpVmp}{Pin} \tag{2.9}$$

- **I-V curve**

The graphical representation of the different parameters that describe the performance of a photovoltaic cell under a given irradiance and temperature levels is known as the I-V curve (**Fig.2.15**). This curve helps to track the maximum power point (MPP) for which the cell can deliver its maximum actual power. Whereas, the fill-factor is the largest square's area under the curve.

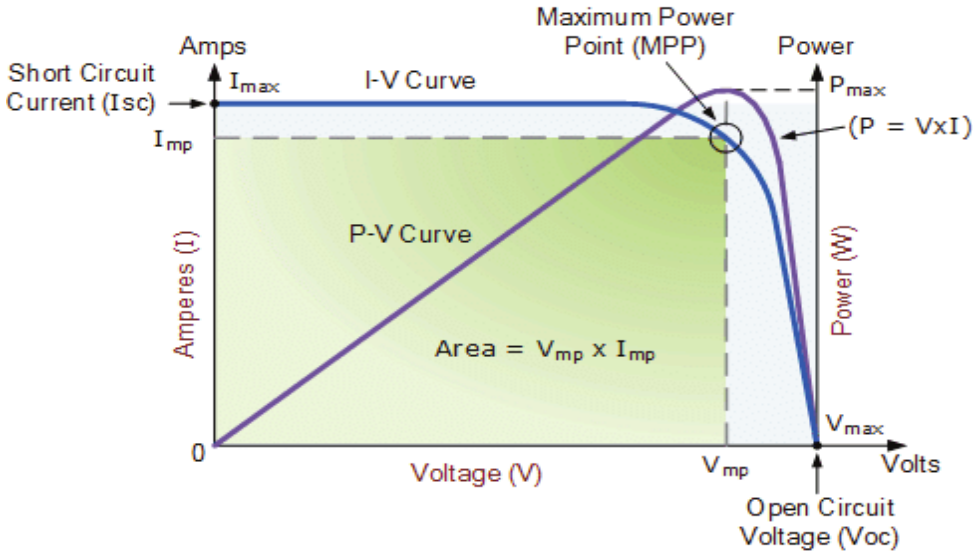

Figure 1.15 I-V and P-V curves

2.3.6 Irradiance and temperature effects

The performance a photovoltaic cell is typically rated using a single operating point at standard test conditions. These conditions are: irradiance of 1000 w/m^2, temperature of 25^{0}C, and 1.5 AM spectrum. However, the efficiency of a PV cell varies in a considerable way with the wide range of real-world operating points. The atmospheric conditions such as the irradiance level and the temperature have a major influence on the behavior of the PV cell.

- **Irradiance level**

The irradiance intensity has a direct effect on the short-circuit current and the generated power, and as a result on the efficiency that decreases with the power dissipation across the

internal resistances (R_{sh}, R_s), while it has a negligible effect on the voltage induced. When the irradiance exceeds a certain level, the efficiency starts decreasing as shown in (**Fig.1.16**).

- **Temperature**

As the temperature of the PV cell increases due to climatic changes or a rise in the heat generated by the internal power losses during the production process, the open-circuit voltage decreases in a notable way. This is in turn affects the efficiency of the cell and the power generated as shown in (**Fig.2.16**).

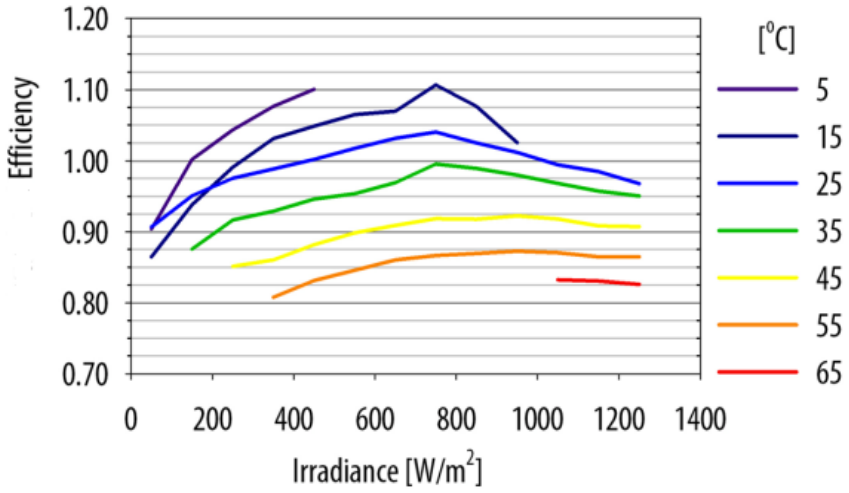

Figure 2.16 Irradiance and temperature effect on the efficiency

3

INSTRUMENTATIONS AND METHODS

3.1 Introduction

The photovoltaic characteristics of a PV cell, module, or an array are driven by the manufacturer under standard test conditions which are an irradiance of $1KW/m^2$ and cell temperature of 25^0 C. However, the environmental and climatic conditions are continuously altering which produces a direct impact on the electrical behavior of the solar modules. For this reason, a real-time virtual data acquisition system is developed to monitor the characteristics and the electrical parameters of a PV module under different test conditions. This system represents a combination of a software environment connected to a microcontroller unit and an electronic load that permits driving the I-V and P-V characteristics curves with more unerring accuracy and lower tracing time. Besides the characterization of the PV module, a software optimizer is developed to extract the one diode model parameters. More details are presented in the coming outlines of this chapter.

3.2 Software Evironment Approach

3.2.1 LabVIEW™

LabVIEW™ which stands for virtual instrument engineering workbench is a software product that has been developed by National Instruments Corporation (NI) to provide an accessible development environment for engineers and scientists. It is used to acquire data and create different automated telemetry systems without writing lines of codes but by using an instead graphical dataflow programming language.

3.2.2 LabVIEW interface for Arduino

Embedded systems exist virtually in every automated application, they represent a combination of an integrated microprocessor, memory, and hardware electrical and/or electronic devices, they are designed to perform a dedicated function in real-time. The real-time operation embedded systems are based on microprocessors with limited and predefined instruction set to perform a specific and a single task with a precise plan; external peripherals are required like the memory chips and the input-output interfaces.[20] However, modern embedded systems are typically based on microcontrollers which are integrated chips that have microprocessors, memories, and interfaces. For this reason, the Arduino AVR microcontroller is used in this project to design and implement our real-time microcontroller-based embedded system. Therefore, the Arduino UNO board which is an electronics

prototyping open-source platform can be interfaced with LabVIEW via LIFA toolkit which makes programming the Arduino with LabVIEW possible instead of writing codes in either C or C++. Labview-Arduino interfacing allows acquiring data from the Arduino microcontroller and processing it in LabVIEW.

3.3 Design The Data Acquision System

3.3.1 Hardware requirements

The real-time data acquisition (DAQ) platform that was implemented and programmed by Ahmed Habes and Amara Ayoub [21] is based on a low-cost Arduino UNO board and on the different sensors that detect the real environmental conditions such as temperature and irradiance and the electrical parameters such as voltage, current and power. The acquired data is then transmitted to LabVIEW through the LIFA interface to plot the I-V and P-V characteristics curves. The block diagram in **Fig.3.1** shows the path of collecting data and transmitting it to be processed.

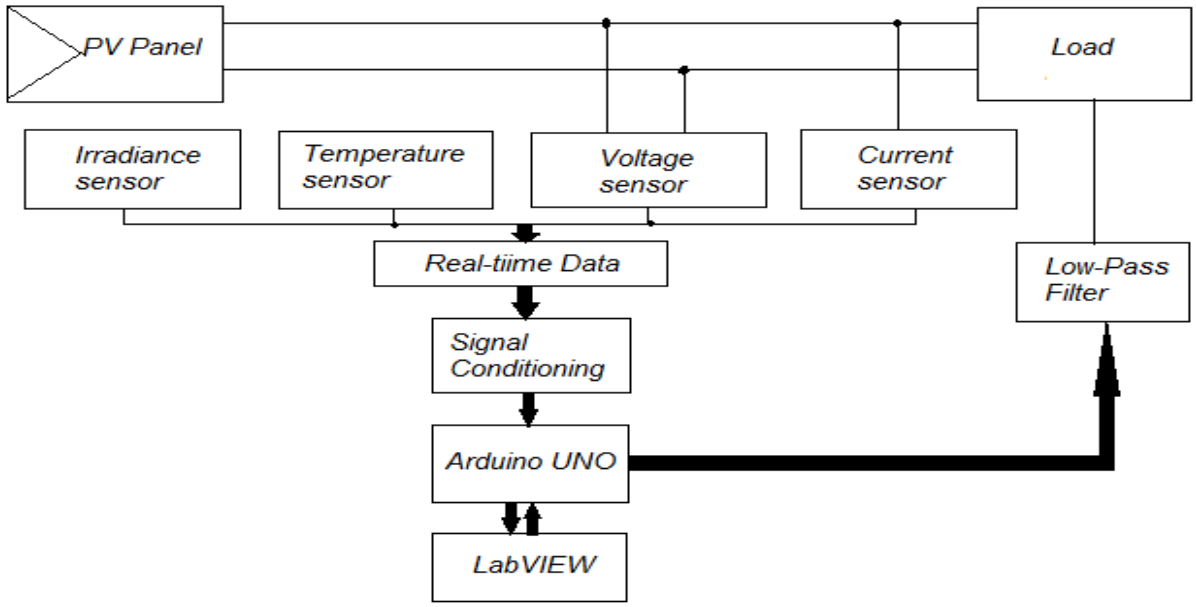

Figure 3.1 block diagram of the PV module characterization platform

- **PV Panel**

Three types of photovoltaic panels are used to test the implemented platform to collect and acquire the PV characteristics under different environmental conditions, and they are as follows:

- SUNTECH_STP080S-12/Bb photovoltaic panel model:

The following table shows the technical data at STC (G=1000 W/m^2; T=25°C; AM=1.5).

Cell technology	Monocrystaline-Si
Rated maximum power (P_{max})	80w
Current at Pmax (I_{mp})	4.65A
Voltage at Pmax (V_{mp})	17.2V
Short circuit current (I_{sc})	5A
Open circuit voltage (V_{oc})	21.6V
Nominal operating cell temperature (T_{NOCT})	50°C
Weight	8Kg
Dimension	1195x541x30 (mm)
Cells number	36

Table 3.1 Technical data of the SUNTECH_STP080S PV module at STC.

Figure 3.2 SUNTECH_STP080S photovoltaic panel.

- SEMTONI_SR05-10W photovoltaic panel model:

The technical characteristics of the SEMTONI_SR05 PV module at STC are in **table 3.2.**

Cell technology	Monocrystaline-Si
Rated maximum power (P_{max})	10w
Current at Pmax (I_{mp})	0.6A
Voltage at Pmax (V_{mp})	16.8V
Short circuit current (I_{sc})	0.68A
Open circuit voltage (V_{oc})	21.0V
Cells number	36

Table 3.2 Technical data of the SEMTONI_SR05 PV module at STC.

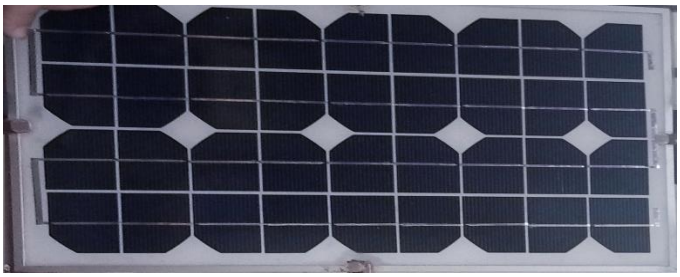

Figure 3.3 SEMTONI photovoltaic panel.

- SUNTECH Md Poly STP050D-12/MEA

The technical characteristics of the SUNTECH Md Poly STP050D-12/MEA PV module at STC are in **table 3.3.**

Cell technology	Polycrystaline-Si
Rated maximum power (P_{max})	50w
Current at Pmax (I_{mp})	2.93A
Voltage at Pmax (V_{mp})	17.4V
Short circuit current (I_{sc})	3.13A
Open circuit voltage (V_{oc})	21.8V
Cells number	36

Table 3.3 Technical data of the SUNTECH Md Poly PV module at STC.

Figure 3.4 SUNTECH Md Poly photovoltaic panel.

- **Arduino UNO board**

Arduino UNO is a programmable open-source microcontroller board based on the ATmega 328P. It has 6 analog input pins and 14 digital input/output pins (of which 6 can be used as a PWM signal generators). The Arduino board in **Fig.3.5** can be powered by a DC power supply that is limited between 6 to 20 volts or through USB connection with computer.

Figure 3.5 Arduino UNO board

- **Signal conditioning circuit**

The KIA324P is a micro-power, low-cost operational amplifier. It is used in the implementation of our DAQ system as a unity gain amplifier (voltage follower) that receives the output voltage of a sensor and then transmits it to the analog read pins of the Arduino Uno board. However, the purpose of using this operational amplifier is to provide an isolation between the sensors and the Arduino and to transfer the same incoming voltage from one high impedance level to another with low impedance.

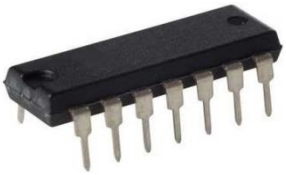

Figure 3.6 KIA324P

- **Power resistor**

A power resistor of 0.3 Ω and 22 W is connected to the negative side of the current sensor to safely convert the highly generated energy into heat. Therefore, it is used for the purpose of protection and controlling power dissipation. [22]

Figure 3.7 Power resistor

- **Voltage sensor**

The instrument voltage transformer used in the implementation of our DAQ system is of a resistive type that works under the voltage divider principle to measure and monitor the DC input voltage induced by the PV module and then reduce it to a range of [0,5V] that is suitable to be read by the analog input pin (A3) of the Arduino.

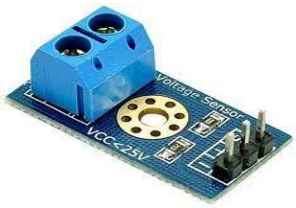

Figure 3.8 Voltage sensor

- **Current sensor**

ACS712-05B-T hall effect current sensor is connected in series with the PV module to detect any variation in the generated DC current. The optimized range of this current transformer varies from - 5A to+ 5A with a sensitivity of 185 mV/A.

Figure 3.9 Current sensor

- **Temperature sensor**

LM35 is an integrated circuit temperature instrument transformer used to return an analog voltage signal that depends proportionally on the centigrade ambient temperature. It provides typical accuracies of ±1/4ºC at room temperature and ± 3/4 ºC over a full – 55ºC to 150ºC temperature range [23]. Therefore, the output voltage of LM35 goes through the KIA324P amplifier to be read by the analog read pin (A5) of the Arduino.

Figure 3.10 LM35 temperature sensor.

- **Load and Low-Pass filter**

The aim of implementing our DAQ system is to plot the I-V characteristics curve under real-time conditions. This process requires a fluctuation and a continuous change in the operating output point of the PV module; this can be achieved by using the IRF740- N-channel MOSFET transistor that is used as a controlled load due to its fast scan to trace the characteristics within less time to reduce the effect of variation in irradiance and temperature. The gate-to-source voltage (V_{GS}) of the MOSFET is controlled via a low-pass RC filter (R=10KΩ and C=4.7µF) that is supplied by a PWM signal of a varying duty cycle from 60% to 80% and generated by the digital-PWM pin (D3) of the Arduino Uno.

(a) **(b)**

Figure 3.11 (a) IRF740- N-channel MOSFET, **(b)** low-pass RC filter circuit

3.3.2 DAQ platform implementation

The scheme of the real-time PV characteristics acquisition system is shown in **Fig.3.12** where all the hardware instruments and devices are connected to the LabVIEW program through the Arduino UNO board.

The complete prototype of the proposed DAQ system is shown in **Fig.3.13**.

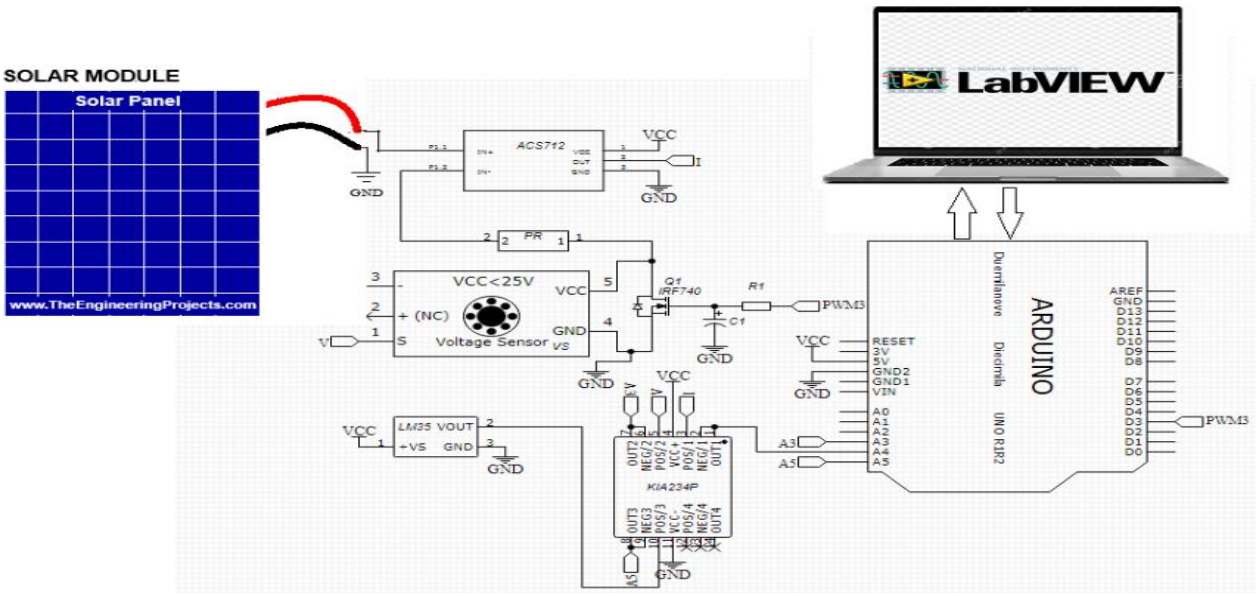

Figure 3.12 The scheme of the DAQ platform

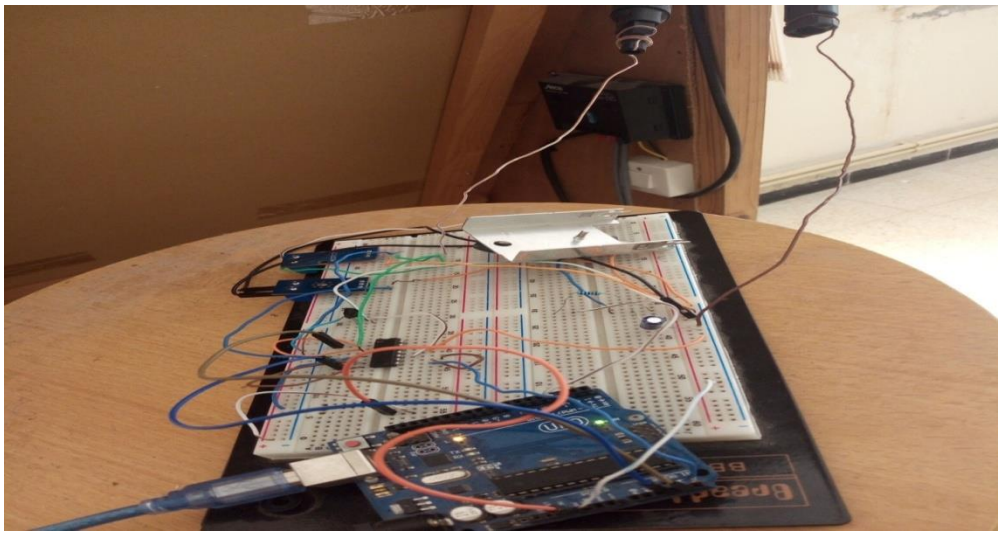

Figure 3.13 The DAQ system

3.3.3 PCB design for the DAQ platform

The scheme in **Fig.3.12** is converted to a printed circuit board (PCB) using the EasyEDA software that allows the realization and the conception of printed circuit boards. A PCB with two layers is selected where the bottom layer is designed for the Arduino Uno board and the top layer for the remaining hardware elements. **Fig.3.14** shows the 3D view of both layers, while **Fig.3.15** shows the routing and the resultant PCB scheme.

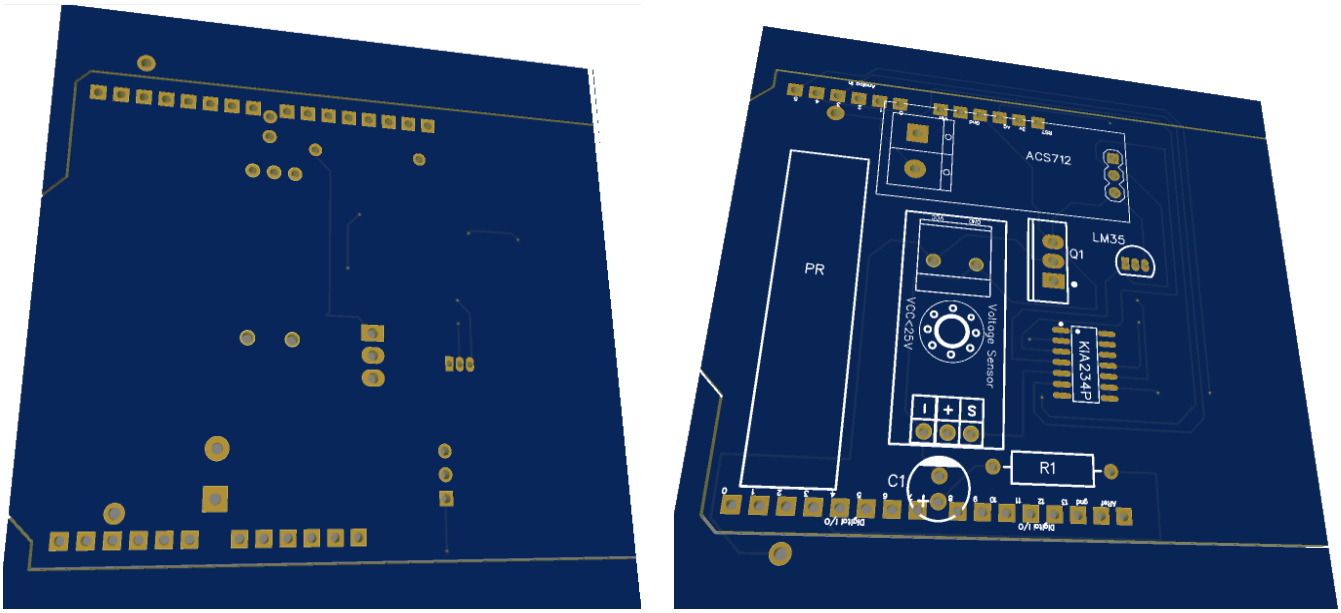

(a) **(b)**

Fig.3.14 3D view of: **(a)** Bottom layer. **(b)** Top layer.

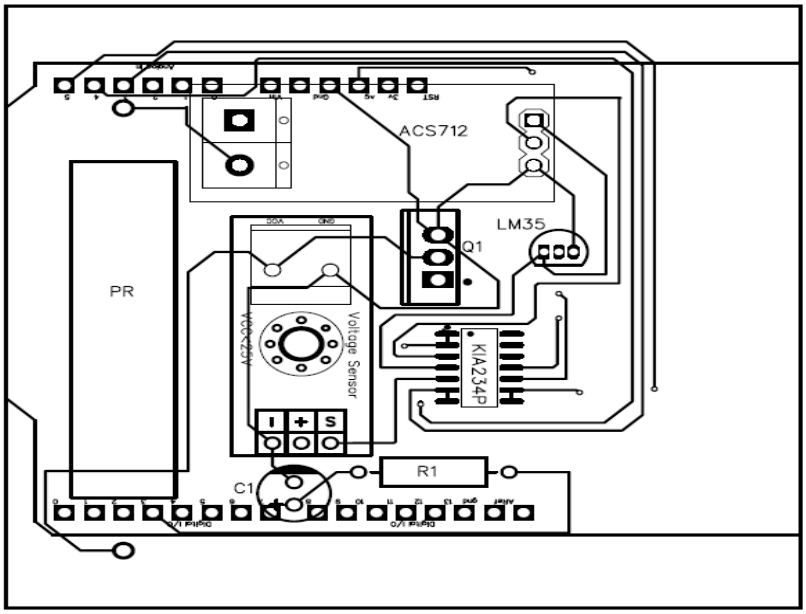

Figure 3.15 Routing of the PCB and the resultant scheme.

3.4 Software Development For The DAQ System

The data acquisition platform based on the Arduino's microcontroller that is implemented in the previous section is programmed using the LabVIEW graphical software environment.

The LabVIEW's front panel in **Figure 3.16** contains two XY graphs to plot the I-V and P-V characteristics curves, while the indicators are used to display the acquired data in real-time.

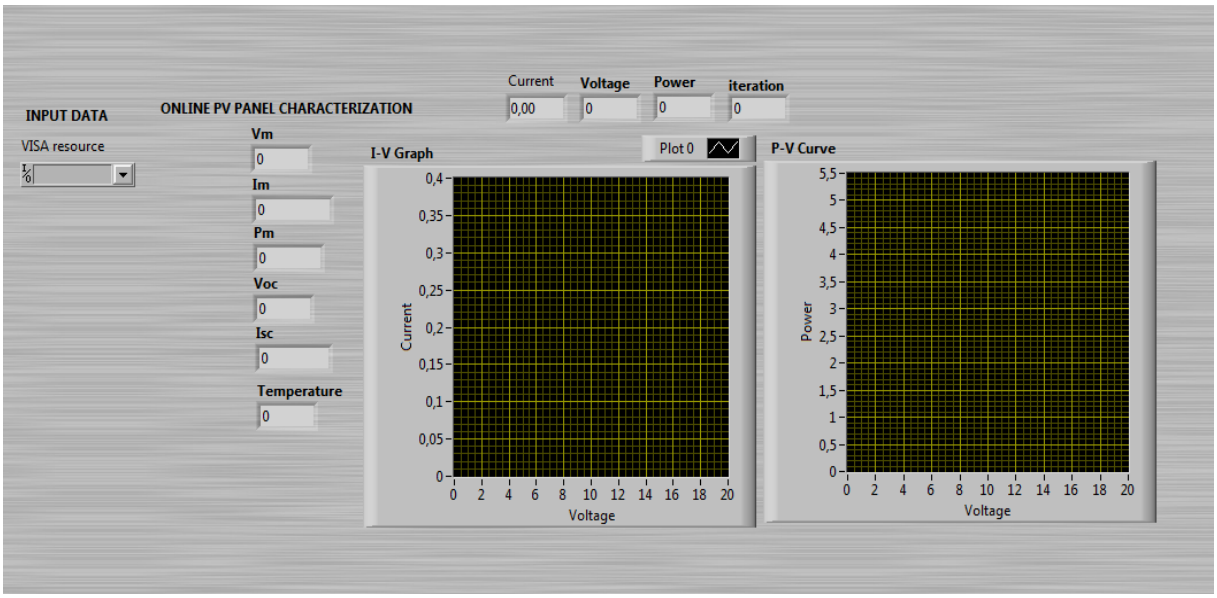

Figure 3.16 LabVIEW's front panel of the DAQ system.

The flowchart in **Fig.3.17** summarizes the steps to collect and plot the estimated data in I-V and P-V curves.

- **Block diagram 1:**

The overview of the LabVIEW block diagram that contains the graphical dataflow software to program the Arduino's microcontroller and process the collected data is shown in page 34.

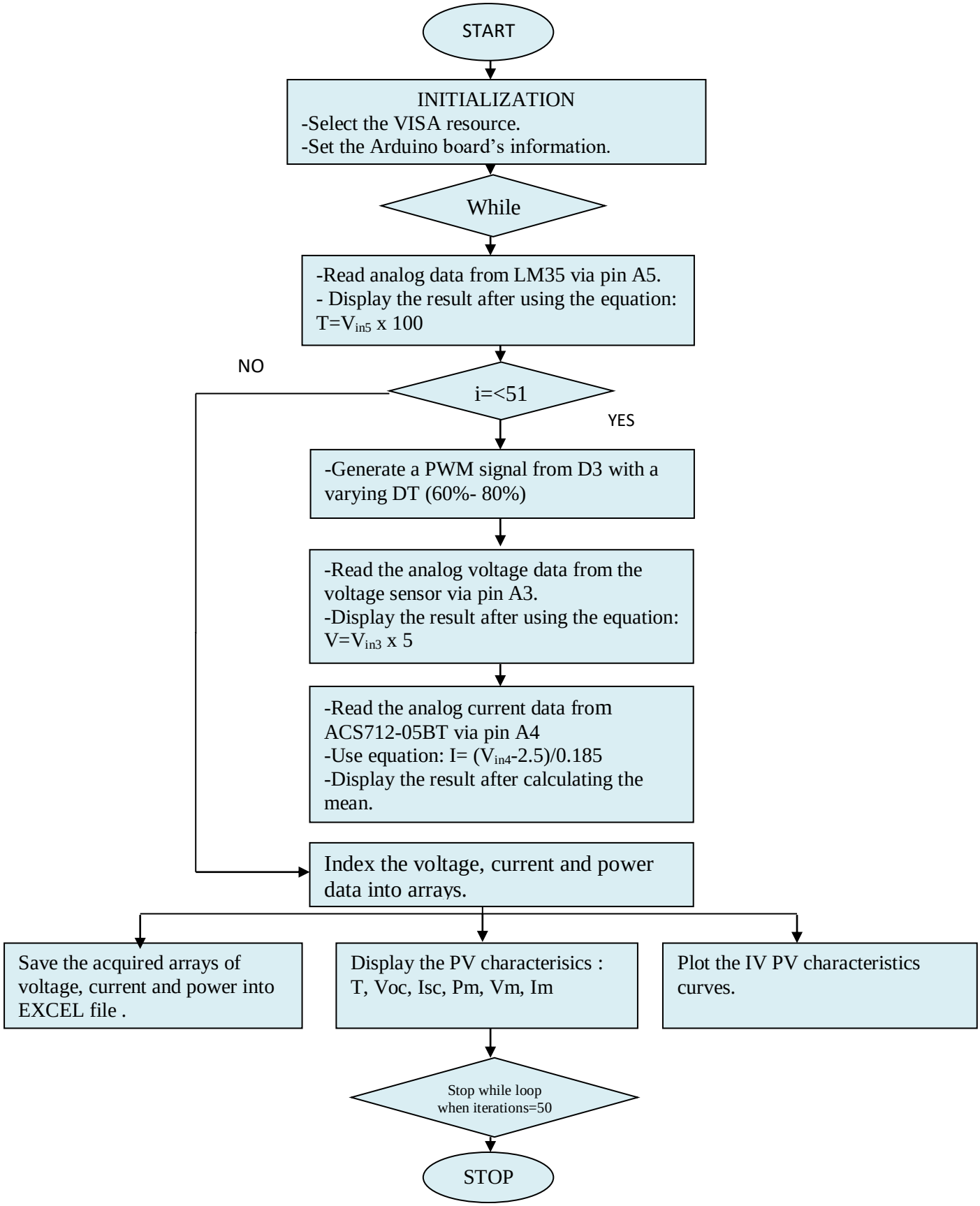

Figure 3.17 The flowchart of the LabVIEW's BD for the DAQ system

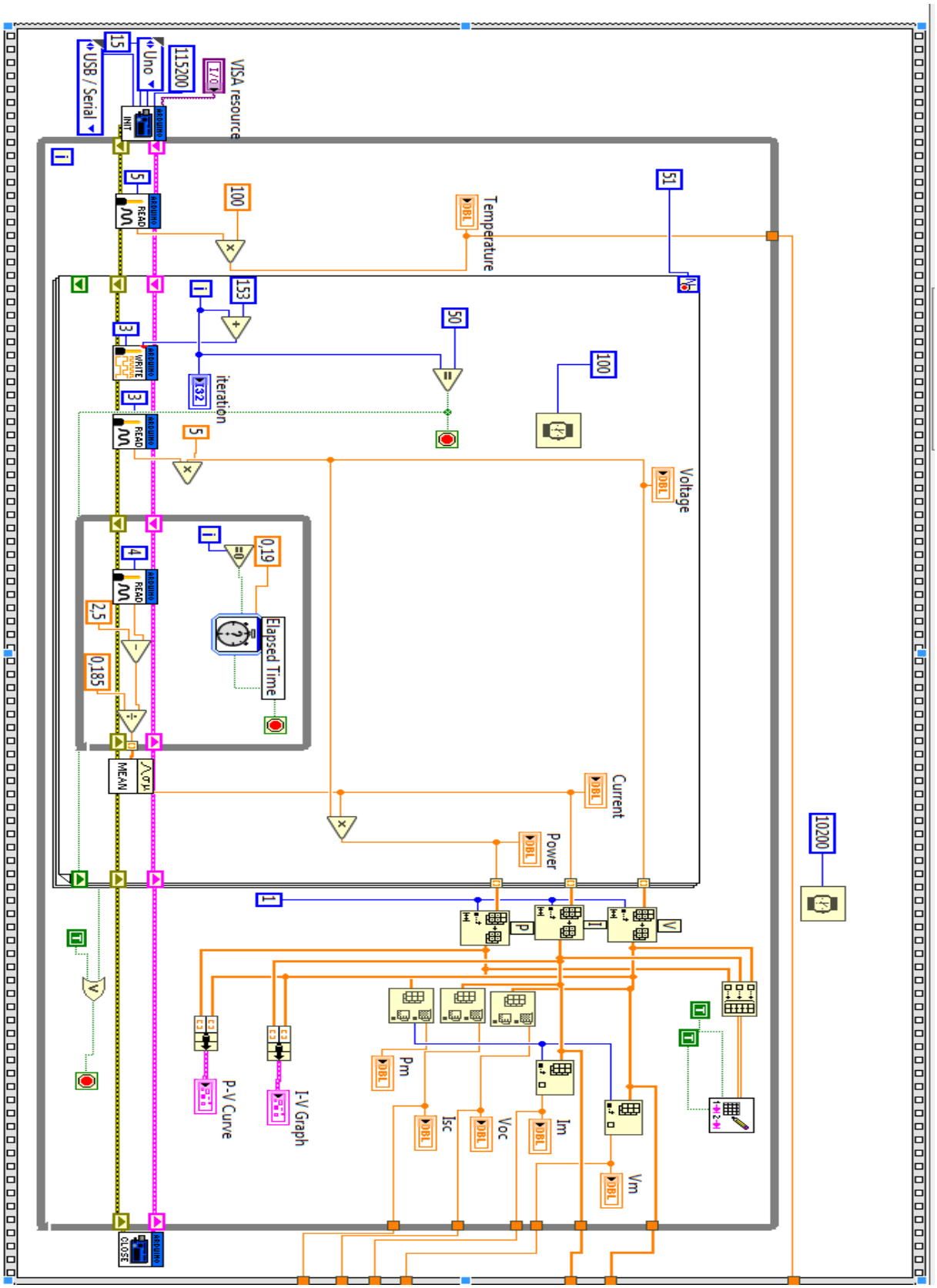
USB / Serial
Uno
115200
VISA resource
Temperature
iteration
Voltage
Elapsed Time
Current
Power
P-V Curve
I-V Graph
Pm
Isc
Voc
Im
Vm
MEAN
10200

3.5 PV Module-ODM Parameters Extraction

3.5.1 Grey Wolf Optimization technique

Real-world problems are characterized by their complexity nonlinearity and a large number of variables which make using the ordinary numerical and analytical methods less efficient in providing more accurate and real results. For these reasons, different meta-heuristic optimization techniques are put in use.

The Grey wolf optimization technique is a bio-inspired and population-based meta-heuristic algorithm that was developed by Mirjalili et al. in 2014. This technique is used for the optimization purposes to simulate and find Optimum search results for the complex and nonlinear real-world functions. This algorithm was inspired from nature based on the social hierarchy and hunting mechanism of grey wolves which are considered apex predators as they are at the top of the food chain. The wolves live in packs where all the members are restricted and committed to the system of social division based on physical strength and hunting strategies. The social hierarchy of grey wolves consists of four levels as explained in the following lines and shown in **Figure 3.18**:

1. Alpha (α) wolves are the leaders of the pack and the responsibles for decisions making and their orders are followed by all members.

2. Beta (β) wolves are the subordinate wolves that stand next to the leader Alpha in decision-making.
3. Delta (δ) wolves submit to Alpha and beta and dominate the Omega wolves.
4. Omega (ω) wolves are the space-goat who submits to all wolves in the pack and they are not considered important individuals and they are the last allowed to eat.

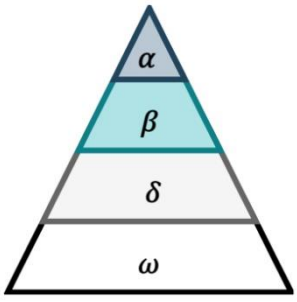

Figure 3.18 Social hierarchy of grey wolves communities

Furthermore, the three major steps of the hunting mechanism based on which the GWO was developed are: exploring and searching for prey, encircling and harassing, and finally

attacking. Each step of the hunting process is described using equations that are included in the GWO algorithm. [24]

The first step is exploring and searching for the prey, represented as:

$$D = |C \cdot X_p - A.X| \tag{3.1}$$

$$X = X_p - A \cdot D \tag{3.2}$$

Where,

X_p : Prey position.

X : Grey wolf position.

A ;C ;D : Coefficient vectors.

However, A and C are calculated as follows:

$$A = 2ar_1 - a \tag{3.3}$$

$$C = 2\,r_2 \tag{3.4}$$

Where,

a : A variable that decreases linearly from 2 to 0.

r_1 and r_2 : Random variables between [0,1].

The second step is encircling and harassing the prey where the α, β and δ wolves locate, surround, and update their positions whenever the prey moves. The ω wolves stay behind to change their locations as they receive the orders. This step is represented in the algorithm as:

$$\begin{aligned} D_\alpha &= |C_1 \cdot X_\alpha - A \cdot X| \\ D_\beta &= |C_2 \cdot X_\beta - A \cdot X| \\ D_\delta &= |C_3 \cdot X_\delta - A \cdot X| \end{aligned} \tag{3.5}$$

$$\begin{aligned} X_1 &= X_\alpha - A_1 \cdot D_\alpha \\ X_2 &= X_\beta - A_2 \cdot D_\beta \\ X_3 &= X_\delta - A_3 \cdot D_\delta \end{aligned} \tag{3.6}$$

$$X = (X1 + X2 + X3)/3 \tag{3.7}$$

The GWO algorithm considers the alpha wolf as the main and the best result attributed to it the accurate prey position. The beta, delta and omega are the second, third and last best solutions.

3.5.2 One Diode Model Parameters Extraction Using GWO

A LabVIEW based optimizer is developed to estimate the five unknown parameters (I_{ph}, I_s, R_s, R_{sh}, n) of the one diode mathematical model that was discussed in chapter 2 using the experimental collected results from the DAQ system which are: T, V, I, V_{oc}, I_{sc}, V_{mp}, I_{mp}. This optimizer is based on the grey wolf algorithm that was updated to extract the ODM parameters by Celina Touabi [25]. The main objective of this optimizer is to minimize the difference between the experimental and theoretical current data, as described in the following objective function.

$$\boldsymbol{F(V,I,Iph,Is,Rs,Rsh,n) = I - Iph + Is\left[e^{\frac{V+I.Rs}{nVtNs}} - 1\right] + \frac{V+I.Rs}{Rsh}} \qquad (3.8)$$

The voltage and current data that is acquired from the DAQ system after 51 iterations is then indexed into 1D arrays and transmitted as input variables to the GWO algorithm.

The thermal voltage Vt is calculated using equation (3.9) and then inputted to the algorithm.

$$\boldsymbol{Vt = \frac{KT}{q} = \frac{1.38.10^{-23} * T}{1.6.10^{-19}}} \qquad (3.9)$$

Where, T is the ambient acquired temperature T_{aq} (°C) that is converted into kelvin ($T=T_{aq}$ (^{o}C) +273.15).

The GWO algorithm requires the definition and calculation of the fitness function for each search agent using equation (3.10). Therefore, the acquired results are compared by evaluating the root mean square error (RMSE) in equation (3.11).

$$\boldsymbol{fitness = \frac{1}{N}\sqrt{\sum_1^N (I\text{-}It)^2}} \qquad (3.10)$$

Where,

N : Population /Search agents / Grey wolves number.

I: Experimental current data.

It: Theoretical current data (equation.2.5).

$$\boldsymbol{RMSE = \sqrt{\frac{1}{N}\sum_1^N F^2}} \qquad (3.11)$$

- **Algorithm pseudocode:**

The GWO based ODM parameters estimation algorithm pseudocode is as follows:

Inputs: T, Vt, Ns, lb, ub, searchagents_no, max_iter, dim,Vm, Im,Voc, Isc

Output: The alpha optimal solution Xα=[I_{ph}, I_s, R_s, R_{sh}, n].

1: Initialization and parameters declaration:

2: Calculate the temperature in kelvin.

3: Calculate the thermal voltage V_t.

4: Set the number of series cells Ns .

5: Enter the current and voltage data that is indexed into arrays.

6: Enter the acquired PV module characteristics (Vmpp, Impp, Voc, Isc).

7: Set the GWO parameters:

8: Set the number of search agents.

9: Set the number of iterations.

10: Define the problem:

11: Set the dimension of the optimal solution's vector.

12: Set the upper and lower bounds of the desired solution.

13: Initialize a, A and C

14: Set α, β, and δ as the first, second, and third best solutions respectively.

15. While i=< max_iteration do:

16: For each search agent

17: For each (V, I)

18: Calculate the objective function.

19: End

20: Calculate the fitness.

21: Update α, β, and δ positions.

22: End

23: Set the solution as global best Xα = [I_{ph}, I_s, R_s, R_{sh}, n].

- **The proposed algorithm's flowchart**

The flowchart that summarizes the GWO based algorithm to identify and extract the ODM parameters is as follows.

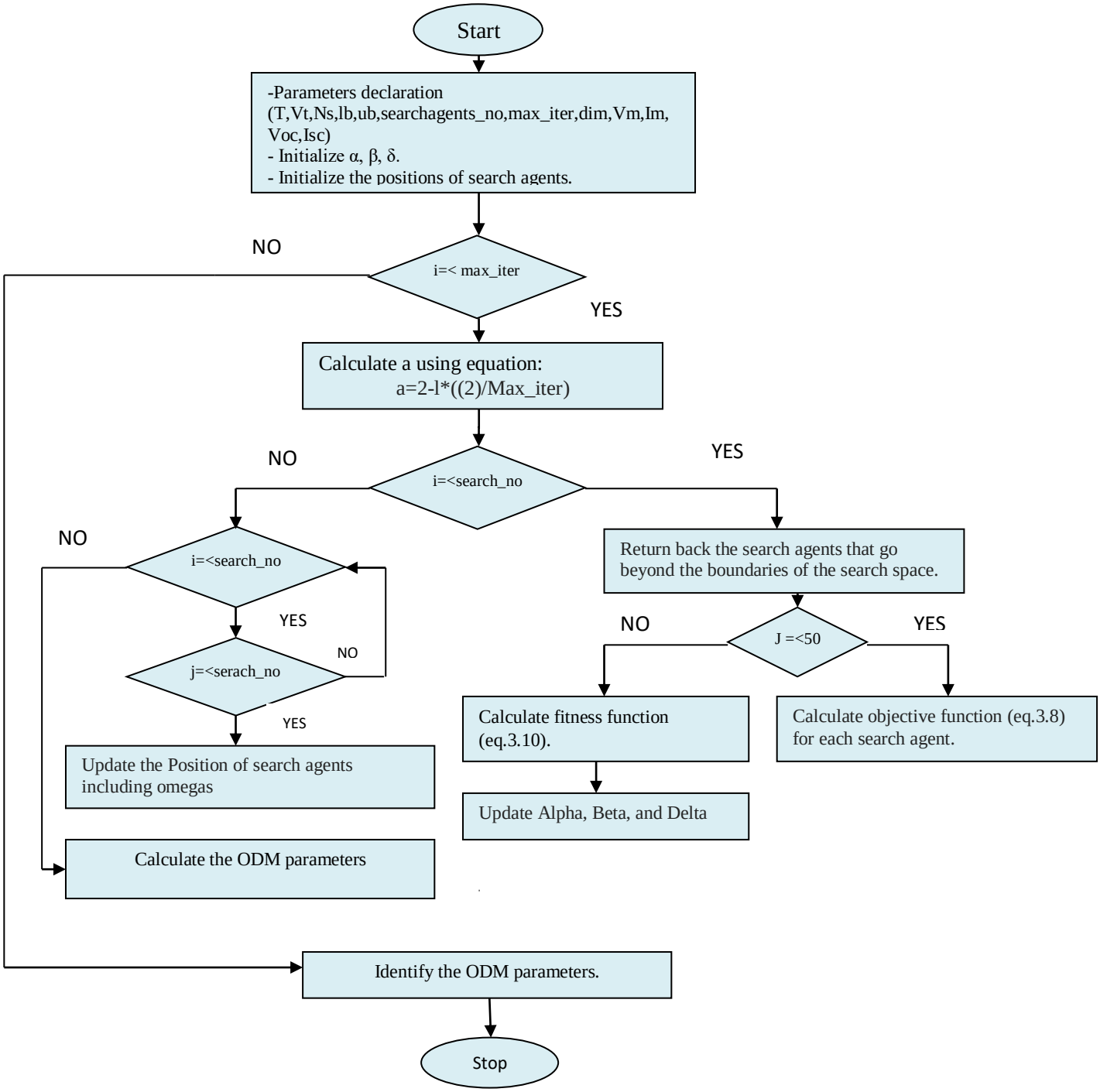

Figure 3.19 The flowchart of the GWO LabVIEW's BD

3.5.3 Software development for the grey wolf optimizer and the combination with the DAQ

The GWO based ODM parameters estimation algorithm is processed in LabVIEW MathScript RT module which is a text-based environment that allows writing functions and scripts and then processing them. The LabVIEW MathScript RT module engine supports some functions that are supported by the MATLAB software so, it permits using text-based scripts created in MATLAB or any other compatible environment [26].

The following figure shows the LabVIEW's front panel of the GWO based parameters estimation block diagram.

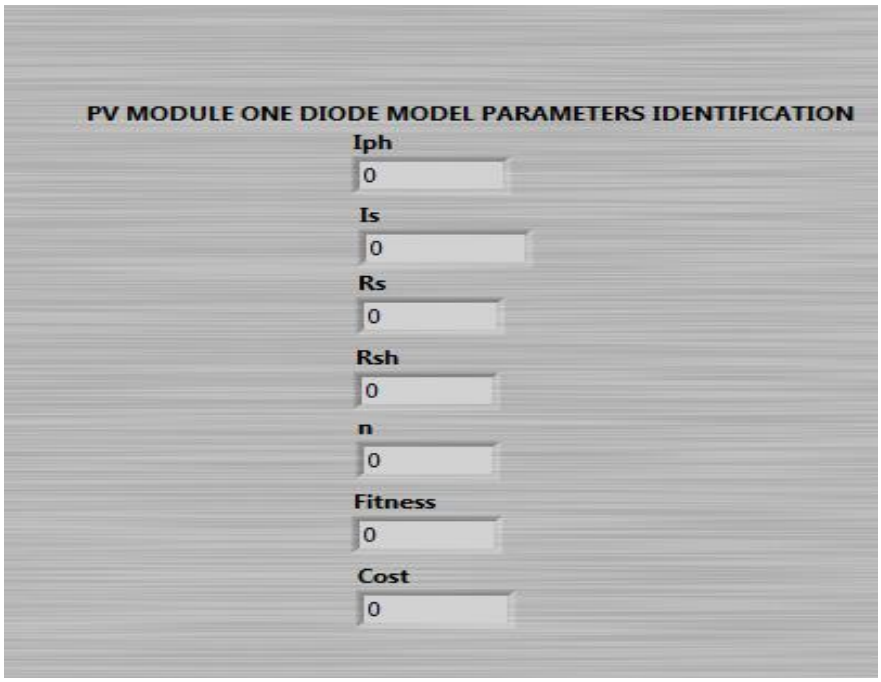

Figure 3.20 Front Panel of the GWO based parameters estimation

- **Block diagram 2:**

The GWO based ODM parameters identification sub-diagram is shown bellow.

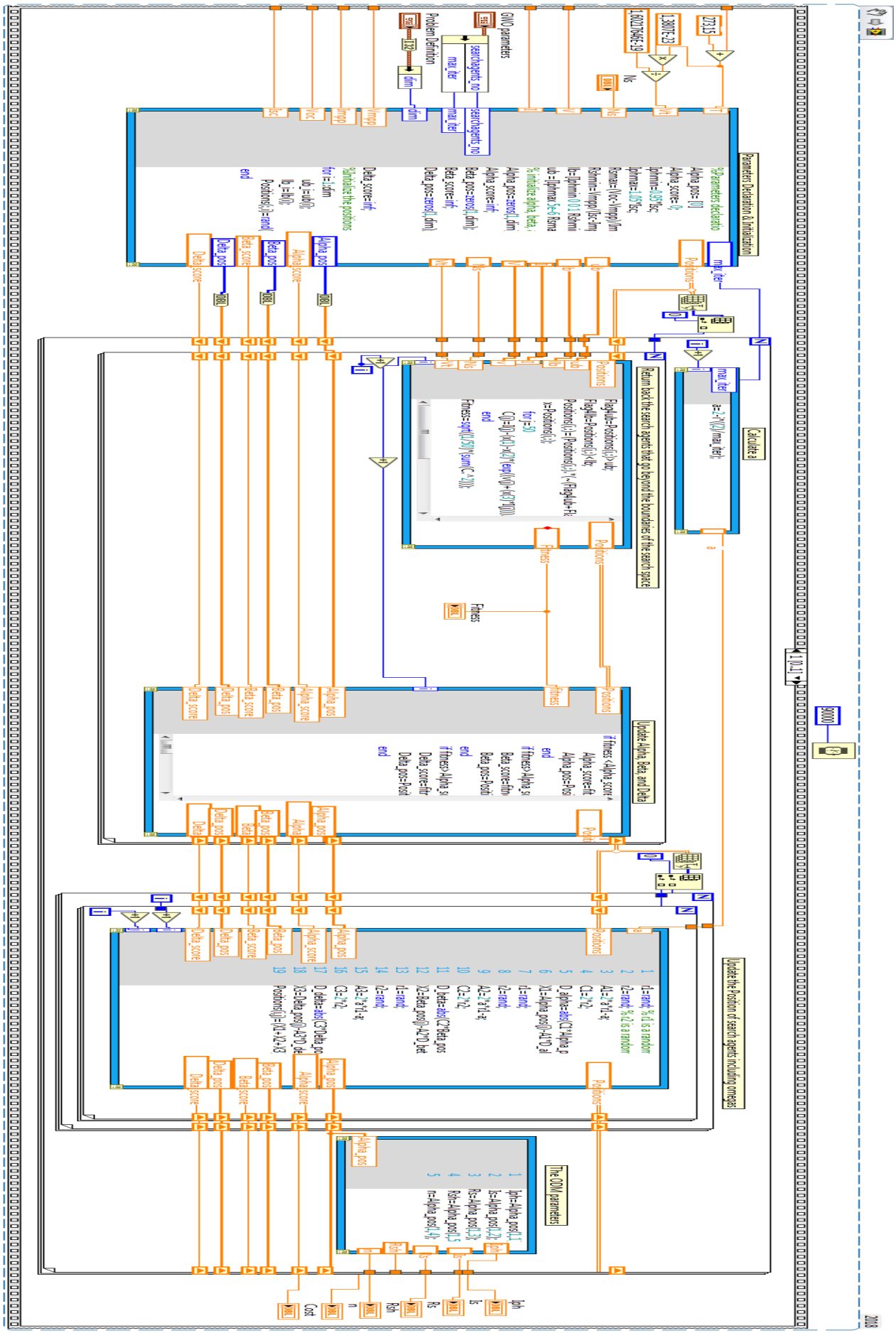
GWO parameters
Problem Definition
Parameters Declaration & Initialization
Return back the search agents that go beyond the boundaries of the search space
Calculate a
Update Alpha, Beta, and Delta
Update the Position of search agents including omegas
The ODM parameters
Alpha_pos
Beta_pos
Delta_pos
Alpha_score
Beta_score
Delta_score
Positions
Fitness
max_iter
Ns
Cost
n
Rsh
Rs
Ls
Iph

- **The complete VI of the characterization and identification system**

The overview of the software's front panel for the DAQ system and the grey wolf optimizer is shown in the following figure. It has four primary parts: the input data, the online PV panel characterization, the I-V and P-V curves, and the PV module ODM parameters identification.

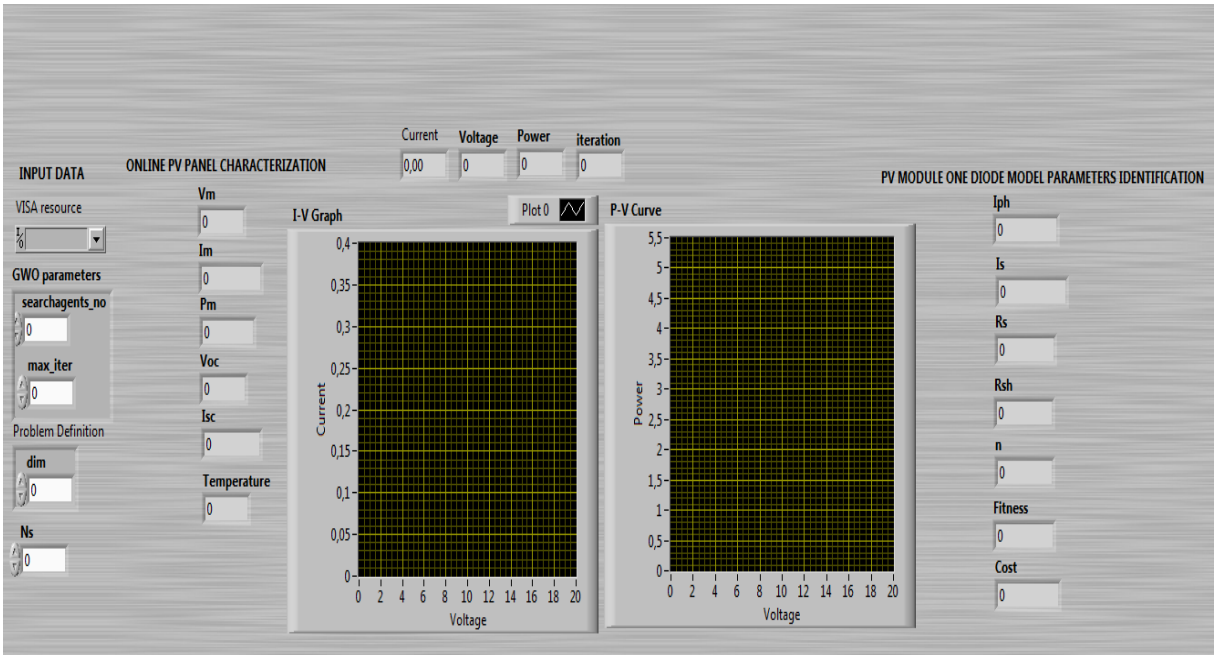

Figure 3.21 The front panel for the DAQ system and the grey wolf optimizer

In the other hand, the DAQ system and the grey wolf optimizer sub-diagrams are combined in the same VI using the flat sequence structure with two frames. However, the aim of using this function is to provide a sequential execution of the two subVIs, which means the input data to the GWO subVI depends on the output of the DAQ system frame. The delay time to execute the first and the second frames is set to be 10200 ms and 90000 ms, respectively.

- **Block diagram 3:**

The complete block diagram of both characterization and identification systems is as shown bellow.

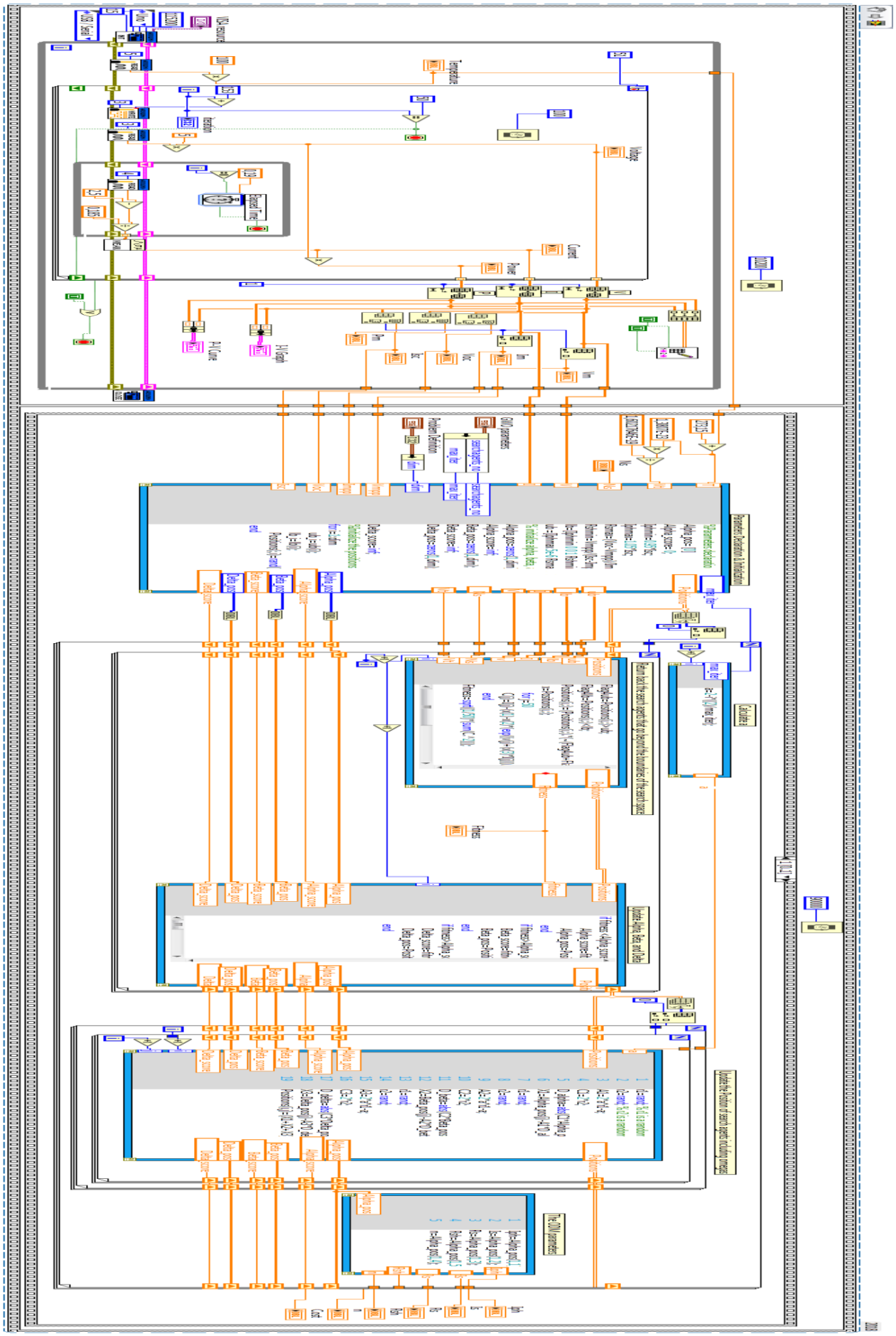

4

TEST RESULTS

4.1 Introduction

This chapter presents the testing procedures and results in order to validate of the LabVIEW based PV characterization and ODM parameters identification under different temperature and irradiance levels.

4.2 Tools Requirements For The System Validation

NI LabVIEW™ 2018(32-bits) software is used as the data acquisition environment on a PC with the following system specifications:

Processor	Intel® Core™ i3 CPU M 380 @ 2.53GHz
RAM	4.00 Go
System type	Exploitation system 64-bits

Table 4.1 Computer's system specifications

The Arduino's AVR microcontroller is programmed using the LabVIEW's VI. Thus, the LIFA activation is required to enable the LabVIEW to detect the VISA resource (COM).

4.3 Testing Procedures

The desired optimal solutions are selected to be within ranges that lead to better accuracy [23], the ranges are shown in **table.4.2**.

Output	**Range**
Iph	[0.95Isc , 1.05Isc]
Is	[0 , 5.10-6]
Rs	$[0, \frac{Voc-Vmpp}{Impp}]$
Rsh	$[\frac{Vmpp}{Isc-Impp}, 1500]$
n	[1 , 2]

Table 4.2 The problem boundaries

The algorithm parameters declaration is presented in **table.4.3**.

Parameters	**settings**
Number of search agents	30
Number of iterations	1000

Table 4.3 GWO parameters declaration

5.4 Test Site Parameters

The tests are performed in the month of June/2022 in Boumerdes, Algeria with the following geographical parameters.

Locality	Boumerdes
Country	Algeria
Latitude (°)	36.76639
Longitude(°)	3.47717
Altitude(m)	9
Time zone	UTC+1

Table 4.4 Geographical site parameters

5.4 Testing Results

Three different photovoltaic modules are used in the implementation and in the testing procedure of the developed LabVIEW based online PV characterization and ODM electrical parameters estimation. The following table shows the main PV characteristics of the three modules under the STC conditions.

PV module	**Cell Technology**	**Pmax(W)**	**Vmax(v)**	**Imax(A)**	**Voc(v)**	**Isc(A)**
SEMTONI SR05	Mono-crystalline	10	16.8	0.6	21.0	0.68
SUNTECH_STP080S	Mono-crystalline	80	17.2	4.6	21.6	5
SUNTECH_STP050D-12/MEA	Poly-crystalline	50	17.4	2.93	21.8	3.13

Table 4.5 PV characteristics of 3 PV modules under the STC conditions.

Case study 1: SEMTONI SR05-10W SOLAFR PV module.

The following LabVIEW's front panel shows the online experimental findings and the I-V and P-V curves under real-time environmental conditions.

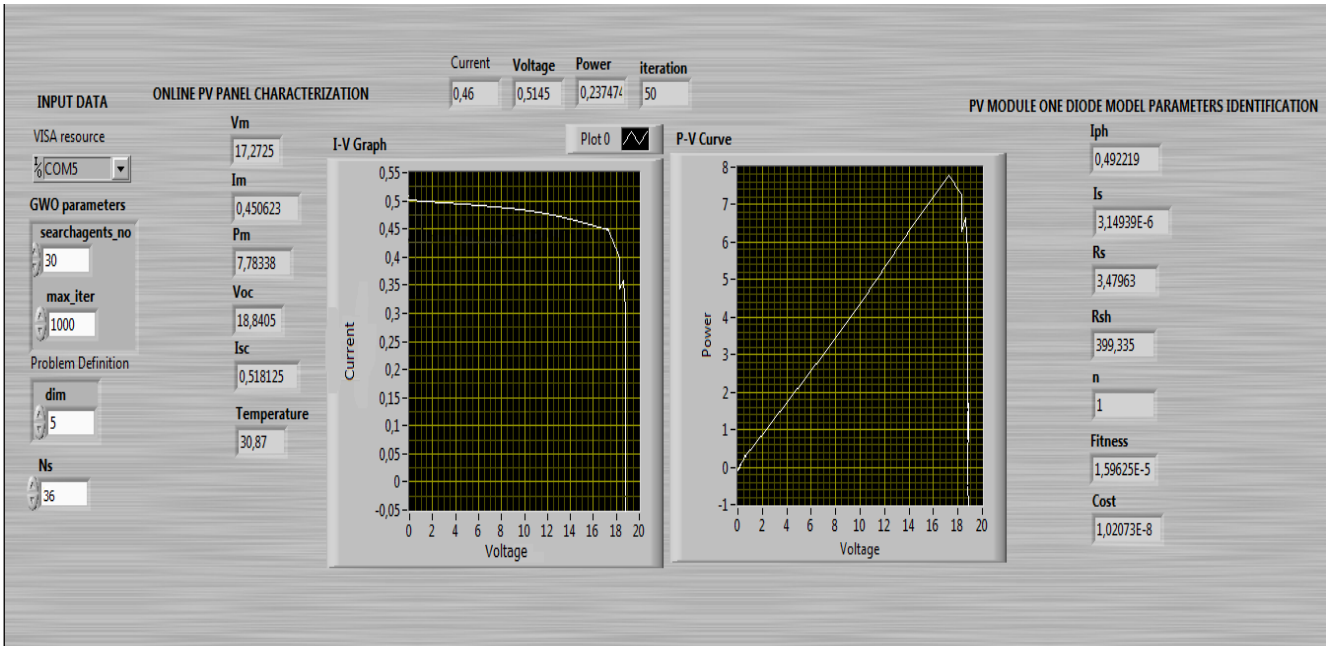

Figure 4.1PV characterization and ODM identification FP of case1.

- **The online PV panel characterization:**

Vm	Im	Pm	Voc	Isc	Temperature
17.2725 V	0.450623A	7.78338W	18.8405V	0.518125A	30.87°C

Table 4.6 PV characteristics of case 1.

- **The PV panel ODM parameters identification:**

Iph	Is	Rs	Rsh	n	Fitness	Cost
0.492219	$3.14939.10^{-6}$	3.47963	399.335	1	$1.59625.10^{-5}$	$1.02073.10^{-8}$

Table 4.7 ODM parameters of case 1.

- **The acquired experimental electrical data:**

The values of voltage, current and power calculated by the DAQ system are presented in **Table 4.8.**

Iterations	Voltage(v)	Current(A)	Power (w)
1	18,816	0,016	0,293
2	18,767	0,031	0,586
3	18,816	0,023	0,441
4	18,767	0,021	0,396
5	18,816	0,015	0,28
6	18,767	0,024	0,45
7	18,791	0,028	0,521
8	18,791	0,024	0,448
9	18,791	0,026	0,491
10	18,791	0,032	0,604
11	18,791	0,012	0,218
12	18,767	0,013	0,248
13	18,84	0,055	1,034
14	18,791	0,04	0,753
15	18,791	0,042	0,799
16	18,791	0,051	0,949
17	18,791	0,065	1,226
18	18,84	0,058	1,091
19	18,791	0,067	1,256
20	18,84	0,09	1,693
21	18,84	0,057	1,081
22	18,791	0,109	2,044
23	18,791	0,101	1,9
24	18,791	0,122	2,3
25	18,791	0,137	2,571
26	18,791	0,151	2,84
27	18,791	0,16	3,006
28	18,791	0,231	4,345
29	18,791	0,233	4,378
30	18,816	0,314	5,899
31	18,816	0,307	5,773
32	18,596	0,358	6,666
33	18,326	0,342	6,276
34	18,277	0,399	7,284
35	17,273	0,451	7,783
36	14,455	0,45	6,505
37	10,216	0,438	4,479
38	7,203	0,429	3,089
39	1,103	0,436	0,481

40	0,784	0,48	0,376
41	0,661	0,458	0,303
42	0,661	0,473	0,313
43	0,613	0,447	0,274
44	0,613	0,457	0,28
45	0,588	0,518	0,305
46	0,588	0,461	0,271
47	0,588	0,466	0,274
48	0,539	0,49	0,264
49	0,539	0,484	0,261
50	0,514	0,462	0,237

Table 4.8 The real-time collected data.

- **Discussions**

The test of the SEMTONI SR05 PV module is performed outdoor under environmental condition with a considerable amount of irradiance and temperature. The acquired voltage, and current measurements are used to draw the well fitted I-V and P-V characteristics which exclude the possibility of notable disturbances or errors that may occur during the online data extraction. The PV experimental characteristics are closer to the ones provided by the manufacturer at STC which affirms the ideality of the surrounded environmental conditions and the manually predicted tilt of the PV module.

The ODM parameters identified by the GWO algorithm and displayed in the front panel (FP) are within the known ranges. However, the difference between the calculated and the measured currents is too small ($1.02073.10^{-8}$) which asserts that the identified parameters are accurate and precise.

<u>Case study 2:</u> SUNTECH_STP080S-12/Bb PV module.

The front panel of the LabVIEW based data acquisition system associated with the grey wolf optimizer when the test is done using the SUNTECH_STP080S-12/Bb PV module is shown in **Fig 4.2**.

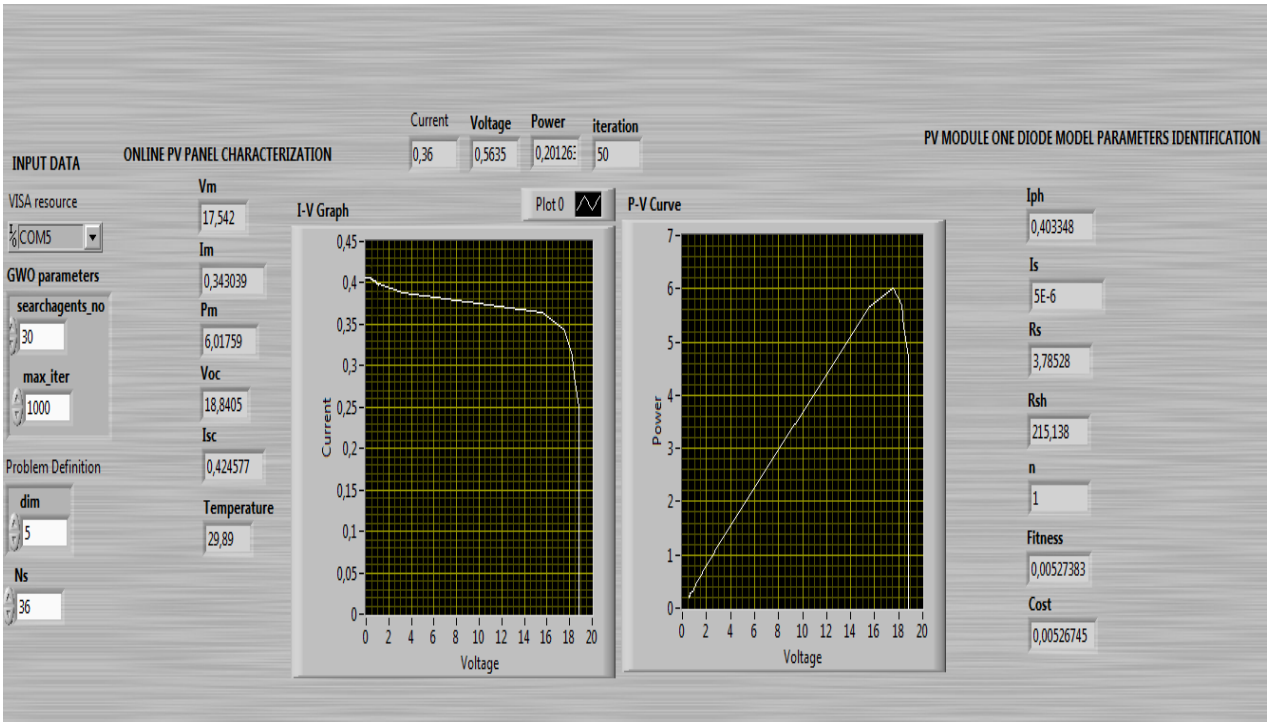

Figure 4.2PV characterization and ODM identification FP of case2.

- **The online PV panel characterization:**

Vm	Im	Pm	Voc	Isc	Temperature
17.542 V	0.343039A	6.01759W	18.8405V	0.424577A	29.89°C

Table 4.9 PV characteristics of case 2.

- **The PV panel ODM parameters identification:**

Iph	Is	Rs	Rsh	n	Fitness	Cost
0.403348	5.10^{-6}	3.78528	215.138	1	0.00527383	0.00526745

Table 4.10 ODM parameters of case 2.

- **The acquired experimental electrical data:**

Iterations	Voltage(v)	Current(A)	Power (w)
1	18,914	0,0006	0,0113
2	18,914	0,002	0,0375
3	18,914	0,0023	0,044
4	18,914	0,0031	0,0592
5	18,914	0,004	0,0756
6	18,914	0,0026	0,0483

7	18,914	0,0017	0,0325
8	18,914	0,002	0,0385
9	18,889	0,0018	0,0341
10	18,914	0,003	0,0561
11	18,914	0,0013	0,0251
12	18,914	0,0015	0,0291
13	18,914	0,0005	0,0092
14	18,889	0,0018	0,0341
15	18,914	0,036	0,677
16	18,889	0,027	0,502
17	18,914	0,023	0,431
18	18,914	0,028	0,529
19	18,914	0,033	0,618
20	18,889	0,036	0,68
21	18,914	0,056	1,067
22	18,914	0,069	1,312
23	18,914	0,072	1,368
24	18,596	0,096	1,782
25	18,179	0,12	2,186
26	18,081	0,129	2,327
27	14,896	0,136	2,029
28	0,76	0,164	0,124
29	0,416	0,156	0,065
30	0,441	0,155	0,068
31	0,269	0,144	0,039
32	0,245	0,128	0,031
33	0,245	0,174	0,043
34	0,245	0,16	0,039
35	0,221	0,139	0,031
36	0,221	0,169	0,037
37	0,221	0,128	0,028
38	0,221	0,162	0,036
39	0,221	0,186	0,041
40	0,196	0,182	0,036
41	0,196	0,161	0,032
42	0,196	0,162	0,032
43	0,196	0,109	0,021
44	0,196	0,186	0,036
45	0,196	0,164	0,032
46	0,196	0,128	0,025
47	0,196	0,128	0,025
48	0,196	0,172	0,034
49	0,171	0,169	0,029
50	0,171	0,135	0,023

Table 4.11 The real-time collected data.

- **Discussions**

The SUNTECH_STP080S-12/Bb PV module is tested using the developed platform in an indoor laboratory with low irradiance. The acquired electrical measurements such as current and voltage are used to plot the well fitted I-V and P-V curves which ensure the absence of disturbances. The maximum power acquired during the test is 6.01759W which is not sufficient in comparison with the rated one at STC; this is due to the small currents drawn by the PV panel when the irradiance level is low.

The best identified ODM parameters can minimize the cost function down to 0.00526745. However, the accordance between the obtained results and the surrounded conditions can be considered as a validation for the proposed system.

Case study 3: SUNTECH_STP050D-12/MEA.

The real-time characterization and parameters identification of the poly-crystalline STP050D-12/MEA after 30 iterations when the Arduino UNO PWM signal is selected to vary from a duty cycle of 60% to 71% is illustrated in the LabVIEW's front panel shown in **Fig.4.3**.

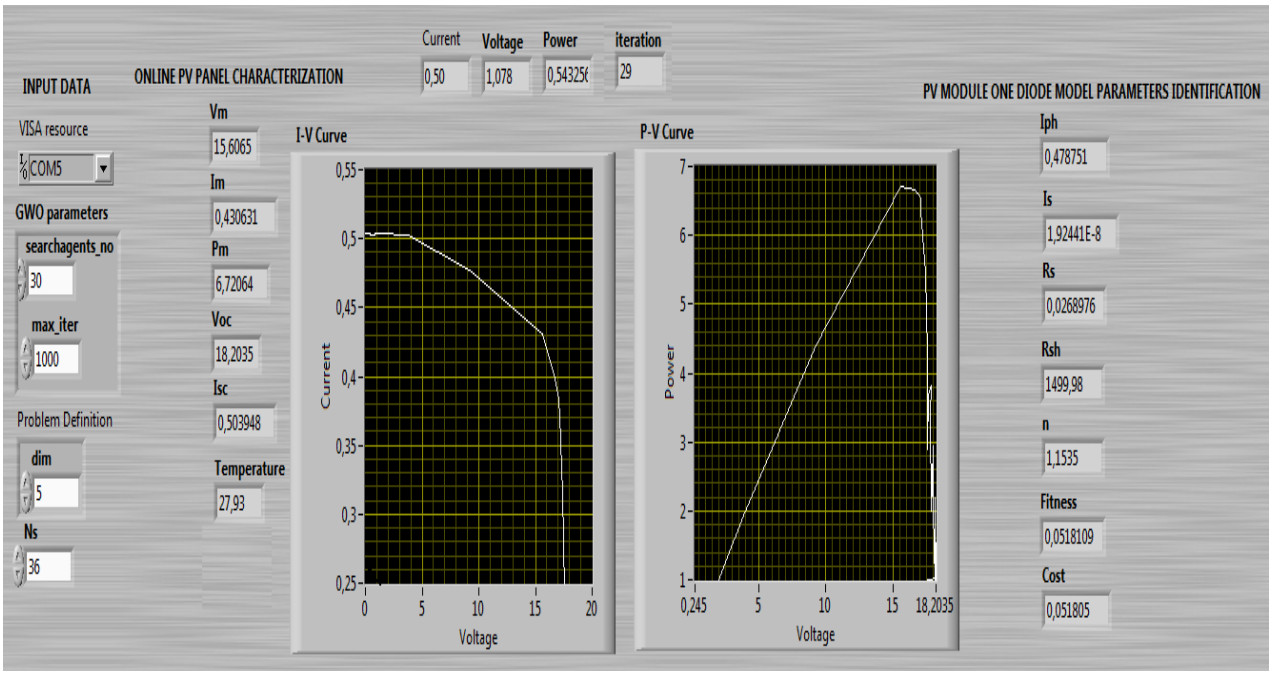

Figure 4.3PV characterization and ODM identification FP of case3.

- **The online PV panel characterization:**

Vm	Im	Pm	Voc	Isc	Temperature
15.6065 V	0.430631A	6.72064W	18.2035V	0.503948A	27.93°C

Table 4.12 PV characteristics of case 3.

- **The PV panel ODM parameters identification:**

Iph	Is	Rs	Rsh	n	Fitness	Cost
0.478751	$1.92441.10^{-8}$	0.0268976	1499.98	1.1535	0.0518109	0.051805

Table 4.13 ODM parameters of case 3.

- **The acquired experimental electrical data:**

Iterations	Voltage(v)	Current(A)	Power (w)
1	18,203	0,057	1,03
2	18,203	0,05	0,914
3	18,203	0,02	0,357
4	18,179	0,048	0,871
5	18,179	0,022	0,405
6	18,179	0,016	0,285
7	18,179	0,084	1,525
8	18,13	0,028	0,504
9	18,13	0,097	1,767
10	18,13	0,079	1,433
11	18,105	0,121	2,192
12	18,056	0,069	1,25
13	18,008	0,126	2,27
14	18,008	0,164	2,951
15	17,934	0,135	2,414
16	17,86	0,112	2,001
17	17,811	0,19	3,385
18	17,836	0,213	3,808
19	17,616	0,208	3,661
20	17,591	0,164	2,889
21	17,591	0,244	4,291
22	17,395	0,315	5,481
23	17,101	0,371	6,349
24	17,052	0,384	6,542
25	16,611	0,401	6,669
26	15,606	0,431	6,721

27	9,187	0,477	4,382
28	3,773	0,503	1,898
29	1,078	0,504	0,543

Table 4.14 The real-time collected data.

- **Discussions**

The SUNTECH_STP050DPV module is tested in an indoor laboratory with an additional light source oriented to the panel. The experimental obtained voltage and current data after 30 iterations are plotted in fitted I-V and P-V curves. However, the PV characteristics are far from the ones at STC due to the low irradiance intensity. In the other side, the ODM parameters that satisfy the minimum of the cost function which is evaluated for this case to be 0.051805 are identified in the front panel in **Fig.4.3**.

The three tests results are conducted using the three different PV modules under different environmental conditions, consequently, this leads to validate the reliability of the developed PC based online acquisition and optimization systems.

5

CONCLUSION AND FUTURE RESEARCH

5.1 Conclusion

This study is considered as a systematic foundation in the field of solar energies as it provides an online monitoring and performance evaluation of the different technologies used in the fabrication of PV modules under real-time conditions of work. However, the proposed method is designed to obtain and acquire the electrical data to plot fitted and I-V and P-V characteristics curves and to drive the technical characteristics under different operation points to have a realistic approach to the overall performances of the PV modules.

The objectives of this research are validated after developing a LabVIEW-Arduino based data acquisition system to collect the voltage, current, and power data of three different PV modules and to compare the obtained real-time characteristics to the ones at STC to evaluate the PV module efficiency. Furthermore, an intelligent meta-heuristics optimization technique is added to the developed LabVIEW block diagram to extract and identify the electrical parameters of the one diode mathematical model which are not driven by the manufacturer. The selected technique is the grey wolf optimization. However, the achieved results show that the identified parameters are considered the best solutions that lead to a minimum difference between the measured and calculated current values. The obtained results show that the developed approach has the ability to provide a smart extraction of the different parameters related to the PV module characterization under different and real-time environmental conditions and to minimize the one diode model objective function to get optimized electrical parameters. Consequently, the effectiveness of this foundation is proved by the best approximation between the acquired real data that are directly influenced by the surrounded conditions and the technical data driven at STC.

5.2 Future Research

This paper presented some developed methodologies that were applied to the PC based characterization platform. Those methods aimed to enhance the performance of the platform to acquire more reliable and accurate results under different real-time conditions. However, future research is required to improve the LabVIEW based data acquisition system to collect more real-time data and then acquire more characteristics using a large number of iterations. Finally, future research should be conducted to focus on finding the electrical parameters of the different PV module's mathematical models using more efficient meta-heuristic optimization techniques.

REFERENCES

[1]. Tomas Markvart, "Solar Electricity". 2nd edition.
[2]. Basu, S.; Antia, H.M, "Helioseismology and Solar Abundances". (2008).
[3]. Tim Sharp; Doris Elin URRUTIA, "How far is earth from the sun?".(2022).
[4]. JOLY Jean-Pierre, "Solar energy: the theoretical bases to understanding it". (2018)
[5]. The Electromagnetic Spectrum, "Why Space Radiation Matters".(8 oct.2019)
Available : https://science.nasa.gov/ems.
[6]. Souilamas Nesrine, "solar radiation". 1st edition, (2017). IFEG/ETB/DPF/ Laboratory ENR.
[7]. Lillesand, T., Kiefer, R. And Chipman, J., "Remote Sensing and Image Interpretation". John Wiley and Sons, NY, 5th ed. (2004).
[8]. Nadine May. "Eco-balance of a Solar Electricity Transmission from North Africa to Europe".(2005)
[9]. Olomiyesan, B.M., Oyedum, O.D., Ugwuoke, P.E., Ezenwora, J.A. and Ibrahim, A.G. "Solar Energy for Power Generation: A Review of Solar Radiation Measurement Processes and Global Solar Radiation Modelling Techniques".(2020)
[10]. Dilip Raja, ''Solar Radiation Measurement Methods using Pyrheliometer and Pyranometer''. (2019).
[11]. The Editors of Encyclopaedia Britannica, "Silicon: chemical element".(22 February 2022)
Available online: https://www.britannica.com/sci-.
[12]. Donald A. Neamen, "Semiconductor Physics and Devices: Basic Principles". 3rd Edition
[13]. Dr. Öğr. Üyesi Abdullah ÜZÜM, "Design and simulation of single, double and multi-layer antireflection coating for c-Si solar cell ".(2019)
[14].Miro Zeman, "Introduction To Photovoltaic Solar Energy".
[15]. Bijit Kumar Dey; " Mathematical Modelling and Characteristic analysis of Solar PV Cell".
[16]. Dorin PETREUS, Cristian FARCAS, Ionut CIOCAN, "Modelling And Simulation Of Photovoltaic Cells".
[17]. Nahla Mohamed Abd Alrahim Shannan, " Single-Diode Model and Two-Diode Model of PV Modules: A Comparison"
[18]. Paththayame Uditha Perera ,Lili He, " A Simplified Mathematical Model for PV Cell Simulation".
[19].Wafaa ABD EL-BASIT, Ashraf Mosleh ABD El–MAKSOOD, " Mathematical Model for Photovoltaic Cells".
[20]. Raj Kamal, " Embedded Systems Architecture Programming and Design". 2nd edition
[21]. Habes Ahmed; Amara Ayoub, "Design and implementation of PV panel characterization platform". (2021)
[22]. "Resistor applications-Power resistor, chapter 5". (2022)
Available: https://eepower.com/resistor-guide/resistor-applications
[23]. "LM35 precision centigrade temperature sensors", Texas Instruments (2017).
Available: https:// ti.com
[24]. Pedro Ponce Cruz ; Arturo Molina Guti´errez ; Ricardo A. Ram´ırez-Mendoza ; Efra´ın M´endez Flores ; Alexandro Antonio Ortiz Espinoza ; David Christopher Balderas Silva,"A practical approach to Metaheuristics using LabVIEW and MATLAB"
[25]. Touabi Cilina," Photovoltaic Cell I-V and P-V Characteristics:Simulation versus Measurement".2021
[26]. "LabVIEW MathScript RT module", LabVIEW help.